Master Thesis

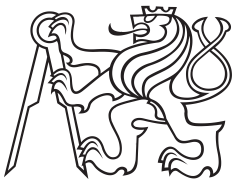

Czech Technical University in Prague

F3

Faculty of Electrical Engineering
Department of elecromagnetic field

Orthomode Waveguide Transducer

Šimon Fojtík

Supervisor: doc. Ing. Pavel Hazdra, Ph.D.
May 2022

ČVUT
ČESKÉ VYSOKÉ UČENÍ TECHNICKÉ V PRAZE

ZADÁNÍ DIPLOMOVÉ PRÁCE

I. OSOBNÍ A STUDIJNÍ ÚDAJE

Příjmení: **Fojtík** Jméno: **Šimon** Osobní číslo: **474234**

Fakulta/ústav: **Fakulta elektrotechnická**

Zadávající katedra/ústav: **Katedra elektromagnetického pole**

Studijní program: **Elektronika a komunikace**

Specializace: **Rádiové komunikace a systémy**

II. ÚDAJE K DIPLOMOVÉ PRÁCI

Název diplomové práce:

Vlnovodný směšovač modů

Název diplomové práce anglicky:

Orthomode Waveguide Transducer

Pokyny pro vypracování:

Seznamte se s principem činnosti vlnovodného směšovače modů - Orthomode Transducer (OMT).
Navrhněte směšovač se vstupem dvou orthogonálních modů TE10 a TE01 (vlnovody WR10) s výstupem na čtvercový vlnovod s přechodem na kruhový trychtýř, případně čtvercový trychtýř se ziskem 20 dBi. K návrhu použijte software FEST3D / CST Studio Suite. Pracovní frekvence OMT by měla být v pásmu 75 - 110 GHz.
Návrh bude probíhat ve spolupráci s firmou RfSpin, s.r.o. (Ing. Zdeněk Hradecký, Ph.D.), pro kterou je určen a která navržený OMT vyrobí a parametry ověří měřením.

Seznam doporučené literatury:

Literatura:
[1] https://ieeexplore.ieee.org/document/6421602
[2] https://ieeexplore.ieee.org/document/6206232
[3] https://ieeexplore.ieee.org/document/6101784
[4] https://ieeexplore.ieee.org/document/5559332
[5] https://www.sciencedirect.com/science/article/pii/S1434841121001953

Jméno a pracoviště vedoucí(ho) diplomové práce:

doc. Ing. Pavel Hazdra, Ph.D. katedra elektromagnetického pole FEL

Jméno a pracoviště druhé(ho) vedoucí(ho) nebo konzultanta(ky) diplomové práce:

Ing. Jan Kraček, Ph.D. katedra elektromagnetického pole FEL

Datum zadání diplomové práce: **30.01.2022** Termín odevzdání diplomové práce: _____

Platnost zadání diplomové práce: **30.09.2023**

[redacted]
doc. Ing. Pavel Hazdra, Ph.D.
podpis vedoucí(ho) práce

[redacted]
podpis vedoucí(ho) ústavu/katedry

[redacted]
prof. Mgr. Petr Páta, Ph.D.
podpis děkana(ky)

III. PŘEVZETÍ ZADÁNÍ

Diplomant bere na vědomí, že je povinen vypracovat diplomovou práci samostatně, bez cizí pomoci, s výjimkou poskytnutých konzultací. Seznam použité literatury, jiných pramenů a jmen konzultantů je třeba uvést v diplomové práci.

10.5.2022
Datum převzetí zadání

[redacted]
Podpis studenta

Acknowledgements

Chtěl bych poděkovat vedoucímu práce panu doc. Ing. Pavlu Hazdrovi Ph.D. a také panu Ing. Zdeňkovi Hradeckému Ph.D. za poskytnutí rad při psaní této diplomové práce. Dále bych chtěl poděkovat své rodině za podporu v době, kdy tato práce vznikala.

I would like to thank my supervisor Ing. Pavel Hazdra Ph.D. and also Ing. Zdeněk Hradecký Ph.D. for providing advice while writing this master thesis. I would also like to thank my family for their support during the time of writing it.

Declaration

Prohlašuji, že jsem predloženou práci vypracoval samostatne, a že jsem uvedl veškerou použitou literaturu.

V Praze, 20. května 2022

I declare that this work is all my own work and I have cited all sources I have used in the bibliography.

Prague, May 20, 2022

Abstract

Orthomode transducers are devices used to separate between two orthogonal waveguide modes generated by received orthogonal polarizations, or to generate these polarizations by routing these modes to the antenna. Their usage effectively doubles the frequency band capacity, since the signals carried by these modes or polarizations do not interfere with each other. Goal of this thesis is to design and measure such device for W frequency band, that could connect to WR10 standard waveguide, integrated with an antenna, using computer simulation and later antenna lab to verify it's function.

Keywords: orthomode transducer, OMT, waveguide, waveguide modes

Supervisor: doc. Ing. Pavel Hazdra, Ph.D.
Department of elecromagnetic field

Abstrakt

Směšovače módů jsou zařízení, která rozdělují dva navzájem kolmé vlnovodné vidy generované přijímanými kolmými polarizacemi, nebo tyto polarizace naopak generují vedením těchto vidů do antény. Jejich použití vede k zdvojnásobení efektivity frekvenčního pásma, signály které tyto vidy či polarizace nesou spolu neinterferují. Cílem této práce je navrhnout a změřit takové zařízení pro W frekvenční pásmo pomocí počítačové simulace a později anténní laboratoře k ověření výsledků.

Klíčová slova: směšovač vidů, vlnovod, vlnovodné vidy

Překlad názvu: Vlnovodný směšovač modů

Contents

Figures

Tables

Orthomode transducer

Orthomode transducer (*OMT*) is a common part of today communications systems. This device separates or mixes two orthogonal modes, which are received or transmitted by an antenna as orthogonal polarizations and effectively increases the utilization of a frequency band. Electrically, we can think about OMT as a passive 4 port device, where the common waveguide carries both orthogonal modes (TE_{10} and TE_{01} in square waveguide, $TE_{11\circ}$ and $TE_{11\bullet}$ in circular waveguide) and therefore provides two electrical ports. Scattering matrix of an ideal OMT device is defined as

$$S = \begin{bmatrix} 0 & 0 & e^{j\Phi_1} & 0 \\ 0 & 0 & 0 & e^{j\Phi_2} \\ e^{j\Phi_1} & 0 & 0 & 0 \\ 0 & e^{j\Phi_2} & 0 & 0 \end{bmatrix}, \tag{1}$$

where ports 1 and 2 belong to the common waveguide and appropriate mods and ports 3 and 4 belong to interfaces for individual modes, rectangular waveguides with dominant mode TE_{10} being most common of these interfaces, fig.1. Ideally, there is zero reflection on all ports, zero transmission between common waveguide ports 1 and 2 and also between ports 3 and 4, perfect transmission from these ports to appropriate common waveguide mode port and zero transmission to the other mode port. In real world designs, these parameters are not achievable and a compromise has to be made.

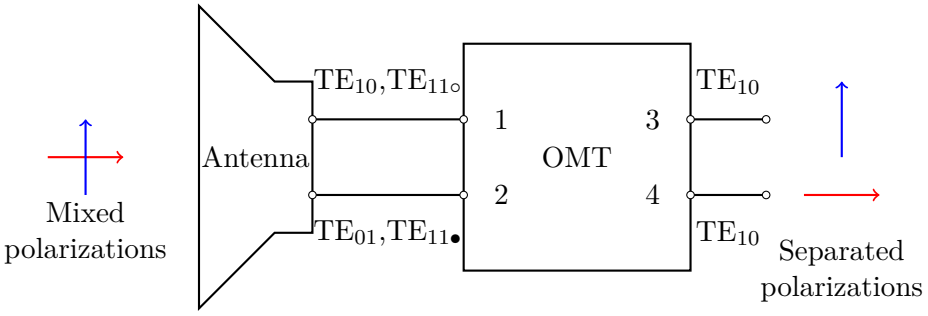

Figure 1: OMT block schematic

In literature [1], [2], [**?**] basic types of orthomode transducers are presented, which have been summarized in the following paragraphs.

Narrowband OMTs

First and most basic of OMTs are narrowband OMTs. These designs aim at good parameters (impedance matching, isolation) only in a narrow frequency band, with fractional bandwidth being around 10%, even though some designs can achieve even bigger bandwidths. While these designs are simple, they are also asymmetrical, which leads to higher order mode generation and therefore lower bandwidth. For some of these designs, variants with direct coaxial port with a probe exist instead of one or both rectangular waveguides, in literature these are called *hybrid OMTs*.

Taper/Branching OMTs

These types of OMTs have the common square or circular waveguide tapered into the rectangular waveguide for one of the modes in the common waveguide. This taper can be either symmetrical, with tapering from both sides, or asymmetrical, with tapering from only one side, fig.2.a. Another waveguide is connected to the side of the common waveguide, which carries the other orthogonal mode, called branching waveguide. Mode TE_{10} in square waveguide or $TE_{11_\circ}$ in circular waveguide can propagate through the tapered section, while mode $TE_{01}/TE_{11_\bullet}$ cannot. Instead, it is reflected back and coupled to the branching waveguide. Placement of this branching waveguide in respect to the tapered section is very important, so that the mode is well coupled and isn't reflected back to the common waveguide. For better impedance match, the branching waveguide is connected to the common waveguide through a short narrowed waveguide section, called an *inductive iris*. The branching waveguide can also be replaced by a coaxial port to get a hybrid OMT design, fig2.d.

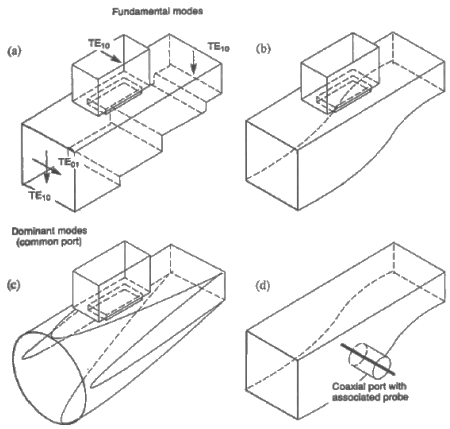

Figure 2: Taper/Branching OMTs, from [1]

Septum/Branching OMTs

The next type of narrowband OMTs are OMTs with a septum. Here, the common square or circular waveguide is split with a septum, which stops mode $TE_{01}/TE_{11\bullet}$ from propagating further. Similarly to previous OMT type, the $TE_{01}/TE_{11\bullet}$ mode is coupled to the branching waveguide or coaxial port, fig.3.a and 3.c. Energy of mode $TE_{10}/TE_{11\circ}$ is spilt on the septum and added together after it. Positioning of the branching waveguide in respect to the septum is also very important for this type of OMT. The septum shape and length are also of great importance, because the shape effects impedance matching (fig.3.b) and the length has to be such, that the $TE_{01}/TE_{11\bullet}$ mode is sufficiently attenuated. This attenuation L can be calculated as

$$L = 20 \log e^{\alpha l}, \tag{2}$$

where α is the attenuation constant of mode $TE_{01}/TE_{11\bullet}$ in the septum region and l is the septum length. To achieve the best performance, the septum should be as thin as possible, in real case this is limited by manufacturing limitations. Impedance matching can further be improved by a capacitive discontinuity in the branching region, fig.3.d.

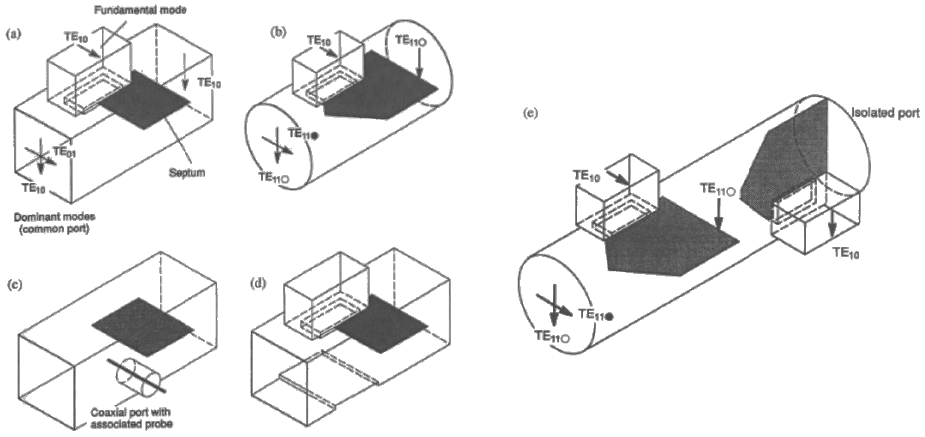

Figure 3: Septum/Branching OMTs, from [1]

Square or circular waveguide behind the septum can be tapered into the rectangular waveguide like in the previous OMT type, by using a taper, or by using two septa (fig.3.e), where the second septum is for good energy coupling to the second branching waveguide.

Acute angle or Longitudinal branching OMTs

In case of acute angle OMTs, the common waveguide is branching under an acute angle from its longitudinal axis into two branches with same/similar profile. Septa are then used in these waveguides, so that only corresponding mod propagates further behind them, fig.4.a and fig.4.b. These waveguides are then transitioned into rectangular waveguides or other interfaces.

Longitudinal branching OMTs (fig.4.c) has both of its branches connected in its longitudinal axis in such orientation, than only the appropriate mode propagates in each branch while the other mode doesn't.

Problems of these OMTs are branching region complexity, where good isolation and impedance matching are hard to obtain.

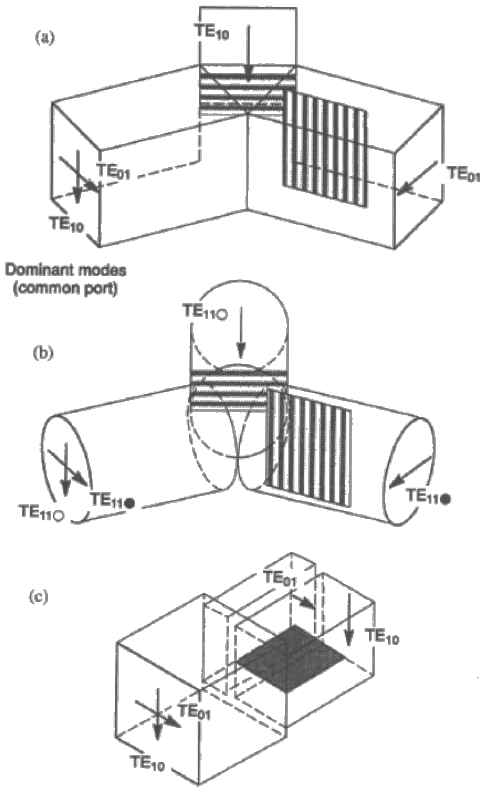

Figure 4: a) and b) Acute angle OMTs, c) Longitudinal branching OMTs, from [1]

Short circuited common waveguide OMTs

The last type of narrowband OMTs is a simple design, where the common waveguide is ended with a short. Rectangular waveguides are than placed perpendicular to the common waveguide in distances $l_{1,2}$ from the short. The distances can be calculated as

$$l_{1,2} = \frac{\lambda_{g1,2}}{4}. \tag{3}$$

$\lambda_{g1,2}$ are the wavelengths of corresponding modes in the common waveguide for center frequency of the operating band. If the common waveguide would not be square or circular for some reason, than also the wavelengths for both modes would differ and the rectangular waveguides would need to be connected at different distances.

In figures 5.a and 5.b, the rectangular waveguides are connected on perpendicular sides of common waveguide and magnetic field component H_z of appropriate mode is coupled as H_x component. In figure 5.c, the rectangular waveguides are connected on the same side, although they can be placed also on opposite sides. In this case, the second waveguide is placed at the short and also in perpendicular orientation, while the first one is placed same as in previous case. The second waveguide now couples the H_x component of $TE_{10}/TE_{11\circ}$ common waveguide mode.

Disadvantage of this type is very narrow bandwidth, which rarely exceeds 10% fractional bandwidth. Advantage is a very easy adaptation to fully coaxial design, fig.5.d.

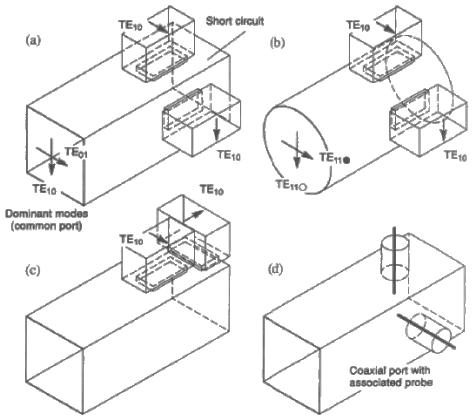

Figure 5: Short circuited common waveguide OMTs, from [1]

Wideband OMTs

For applications that require it, types of OMTs exist, that can achieve 90% fractional bandwidth. Even though bigger bandwidth can be achieved by using ridged waveguides in narrowband designs, their performance isn't the best due to. To improve parameters, a different approach to design has to be taken. Narrowband OMT designs lacked symmetry for one or both of the dominant modes in the common waveguide. Wideband OMTs utilize high symmetry for both modes, which leads to designs that use 2 ports for each dominant mode in common waveguide. After recombining these ports, energies of dominant modes are added and the mode propagates, while energies of higher order modes of common waveguide are canceled out. This effectively increases single mode operation bandwidth.

Bøifot junction

One of wideband OMT types is Bøifot junction, fig.6.a. Energy of TE_{10} mode is split between ports P_1 and P_2, while TE_{01} mode is split between ports P_3 a P_4. For common waveguide mode TE_{10}, ports P_3 and P_4 act as a H-plane T-junction and energy can't couple to these ports up to their cutoff frequency of mode TE_{01}, whereas ports P_1 and P_2 act as a E-plane T-junction and energy can couple to them from their TE_{10} cutoff frequency. The case is same for common waveguide mode TE_{01}, which can't couple to ports P_1 and P_2 but can to ports P_3 and P_4.

After separating the polarizations, it is necessary to again combine corresponding ports by using power combiners or magic tees. By doing this we obtain full power from dominant modes of common waveguide, because modes in the rectangular waveguides are in phase when combined, while modes generated by higher order common waveguide modes are out of phase and are canceled out. Ports P_1 and P_2 are always combined after the septum, so the only thing left is to taper the square waveguide into rectangular one. To combine ports P_3 and P_4, E-plane (fig.6.c) or H-plane (fig.6.d) waveguide bends can be used to bring them together to combine. While E-plane bends are more broadband, H-plane allow for more compact design. Impedance matching is done by shaping the septum and by adding capacitive posts to the side ports. At higher frequencies, thickness of both septum and the posts becomes a problem from manufacturing and mechanical perspective. This can be solved by using thicker spectrum and symmetrical E-plane steps (fig.6.b) and by omitting the posts entirely and instead using capacitive waveguide steps in the sidearms [5],[4].

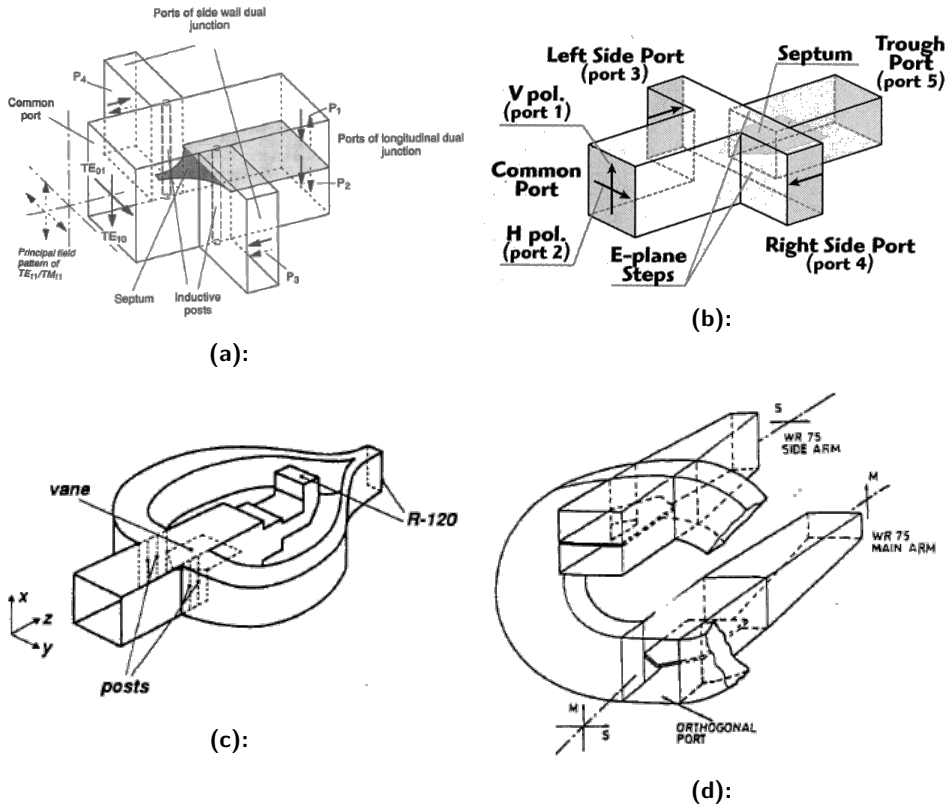

Figure 6: Bøifot junction, a) from[1], b) from[4], c) and d) from[2]

Turnstile junction

This type of OMT, similar to Bøifot junction, again has 2 ports for each common waveguide dominant mode, between which energy is spilt equally. The name of this design comes from its shape, which resembles a turnstile (fig.7.a), even though both square and circular common waveguide can be used. Unlike Bøifot junction, it treats both both dominant modes exactly the same, which means it has four-fold symmetry. It does not need any septums or posts but it does usually have some kind of pyramidal structure for better impedance matching and splitting the modes into the waveguides. Design of this structure can be quite complicated and many different types of them exist, for example in [3] or [7]. The whole assembly gets quite complicated, and several E plane and/or H plane bends need to be used to combine the appropriate ports, which enlarges the OMT quite a but, fig.7.b.

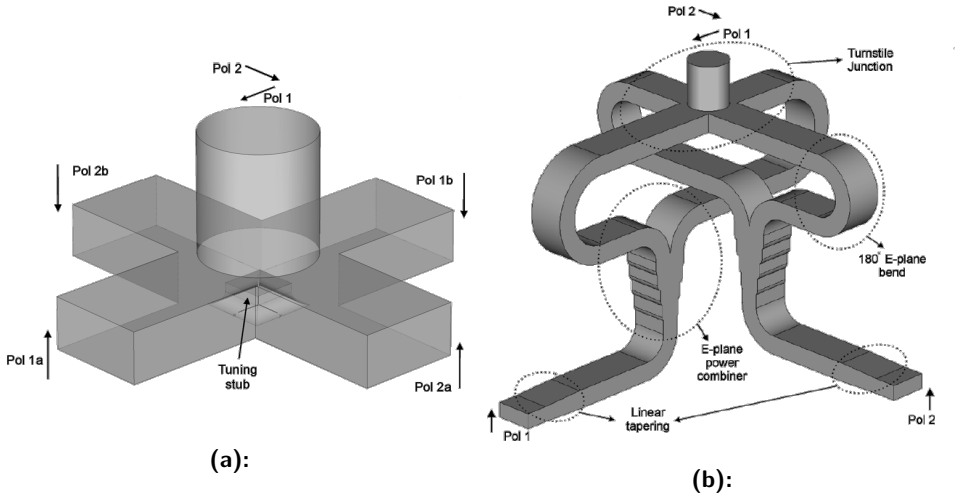

Figure 7: Turnstile junction, from [3]

Finline and quad-ridged OMTs

Finline and quad-ridged OMTs are wideband OMT designs, that get their proprieties from using ridged waveguides, instead of focusing on symmetry.

The finline OMT (8).a consists of a common waveguide that has a pair of diametrically opposite tapered metallic fins, which confine the energy of one dominating common waveguide mode, that has polarization parallel to these pins, to the small gap between these fins. Then the energy is guided out of the common waveguide by a curve in the fins through the side of the waveguide. The other dominant mode passes through the fins and continues down the waveguide. Higher order modes excited by termination of the fins can be suppressed by placing a resistive card at the end.

The quad-ridged OMT (8.b and 8.c) works in a similar manner, where energies of both dominant modes are confined in gaps between orthogonal pair of ridges. These ridges widen the separation between fundamental mode and first higher order modes and effectively increase the bandwidth. The energy of dominant modes is extracted by coaxial probes.

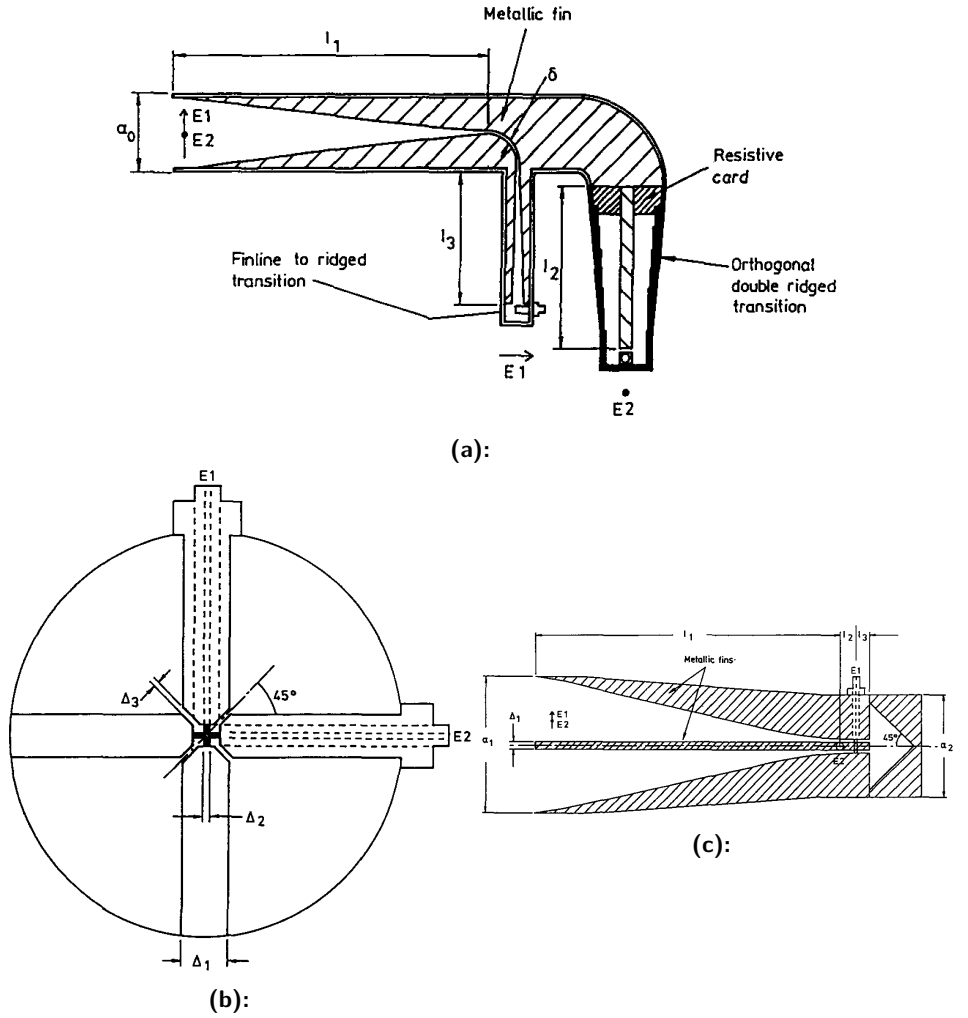

Figure 8: a) Finline OMT, b) and c) Quad-ridged OMT, from [9]

Designing the OMT

Assignment asks for an OMT design with a square common waveguide, working across 75 GHz to 110 GHz, which is the W frequency band, with WR10 standard waveguide outputs. The OMT will be than connected to a conical horn or pyramidal horn antenna with a gain of at least 20 dBi. To cover the whole waveguide bandwidth, which is nearly 40 % fractional bandwidth, the chosen design needs to be wideband.

Design tools

The whole design was done in CST Microwave studio with help of FEST3D software for designing some of the parts. In CST microwave studio software, the whole structure was simulated with help of both Time Domain Solver, which uses finite integration technique (FIT) and Frequency Domain Solver, that uses Finite Element Method (FEM). This software also has a built in optimizer, which can easily be used to tune the performance of the design.

Design process

Even though the assignment is to design the OMT for W frequency band, after discussion it was decided to design the OMT for Ka frequency band (26.5 to 40 GHz) in such a way, that it could be easily scaled, since the fractional bandwidths of both bands are very similar around 40 %.

$$f_{W,lower} = 75\,\text{GHz},\ f_{W,upper} = 110\,\text{GHz}$$
$$f_{W,center} = 92.5\,\text{GHz}$$
$$B_W \doteq 37.8\,\%$$
$$f_{X,lower} = 26.5\,\text{GHz},\ f_{X,upper} = 40\,\text{GHz}$$
$$f_{X,center} = 33.25\,\text{GHz}$$
$$B_X \doteq 40.6\,\%$$

OMT for this lower frequency band can be more easily manufactured and measured, but proves that the design works. The structure dimensions can

than be scaled by factor given by the width dimension of waveguides for corresponding bands.

$$factor = \frac{w_{WR28}}{w_{WR10}} = \frac{2.54\,\text{mm}}{7.112\,\text{mm}} \doteq 0.357$$

Dimensions of the W frequency band OMT will be roughly one third of the X frequency band OMT, this needs to be kept in mind when designing, so that the final dimensions don't get unreasonably small, which could cause problems with manufacturing and mechanical stability.

OMT design

Since a wideband OMT type is needed, Bøifot junction type OMT was chosen for its compact design and reasonable manufacturing difficulty. As mentioned earlier, the OMT should have such dimensions, that it can be easily scaled for higher frequency bands. As can be seen in [6], the traditional approach to designing this OMT for high frequencies leads to very thin capacitive pins and thin septum. This makes it hard to manufacture precisely and complicates the assembly. Therefore, approach similar to ones in [4] and [5] was chosen. The axial port consists of thick septum and symmetrical E-plane steps, while the side ports include capacitive waveguide steps instead of the pins. As motioned before, the final OMT can be thought of as a 4 port device, with 2 ports being provided by the common waveguide dominant modes. In CST, we obtain such S-matrix

$$S = \begin{bmatrix} S_{1(1)1(1)} & S_{1(1)1(2)} & S_{1(1)2(1)} & S_{1(1)3(1)} \\ S_{1(2)1(1)} & S_{1(2)1(2)} & S_{1(2)2(1)} & S_{1(2)3(1)} \\ S_{2(1)1(1)} & S_{2(1)1(2)} & S_{2(1)2(1)} & S_{2(1)3(1)} \\ S_{3(1)1(1)} & S_{3(1)1(2)} & S_{3(1)2(1)} & S_{3(1)3(1)} \end{bmatrix}.$$

Ports 2 and 3 are single mode, so we can see them as 2(1) or 3(1) in this matrix. Port 1 has two modes, that correspond to 1(1) for TE_10 mode and 1(2) for TE_01 mode. Port 2 is the axial port and should have good transfer to port 1(1), port 3 corresponds to the combined side ports and should good transfer to port 1(2). Other goals of this design are to minimize return loss at all ports and minimize transfer between other port combinations.

Base structure design

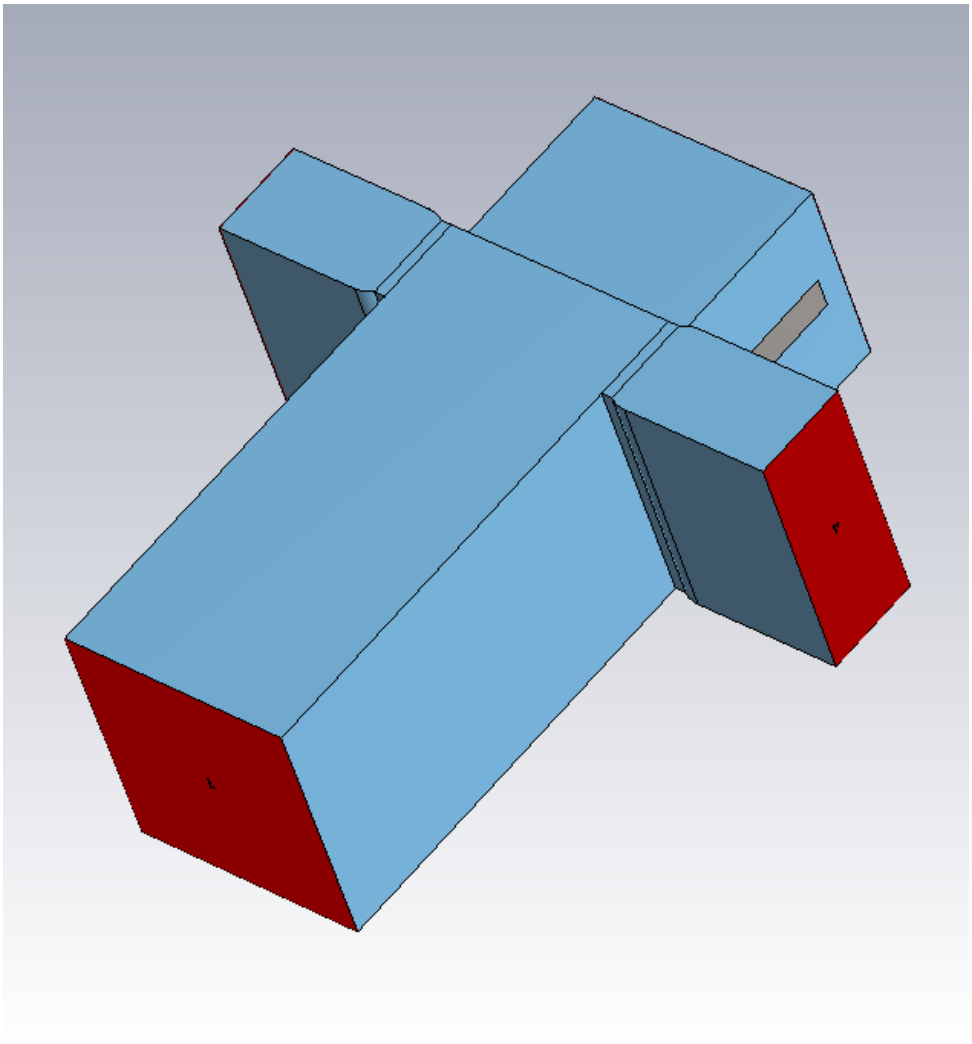

Figure 9: OMT base structure

The first step was to design the base structure of the OMT, which means common waveguide, axial port with septum and side ports with capacitive irises. The standard waveguide used for Ka frequency band is WR28 with dimensions $a = 7.112\,\text{mm}$ by $b = 3.556\,\text{mm}$, which is the same ratio as WR10 waveguide. By choosing the square waveguide dimensions same as a, we obtain greatest possible bandwidth and also make designing the latter transformers easier, since they will need to change only in one dimension. The septum shape should be such, that it acts like a bend from the common waveguide to the side ports for the TE_{01} mode at its E field maximum, shown in figure 10.c. Two septum shapes were simulated, one with a smooth bend defined by an arc with a radius and one with several breaks connected by straight lines, both shown in figure 10.b. There was little to no difference between

effect of shape on the TE_{10} mode, as can be seen in figure 10.a, where this mode is labeled as (1) and corresponding s-parameter is $S_{1(1)1(1)}$. The main effect of shape was on the TE_{01} mode, as expected, labeled as (2) which corresponds to $S_{1(2)1(2)}$. The shape with breaks performed slightly better, therefore following designs include this shape. Other parameters, like transfer between single mode ports and cross-polarization discrimination also turned out very well for this design. The side arm waveguides have slightly lower height than the output WR28 waveguides.

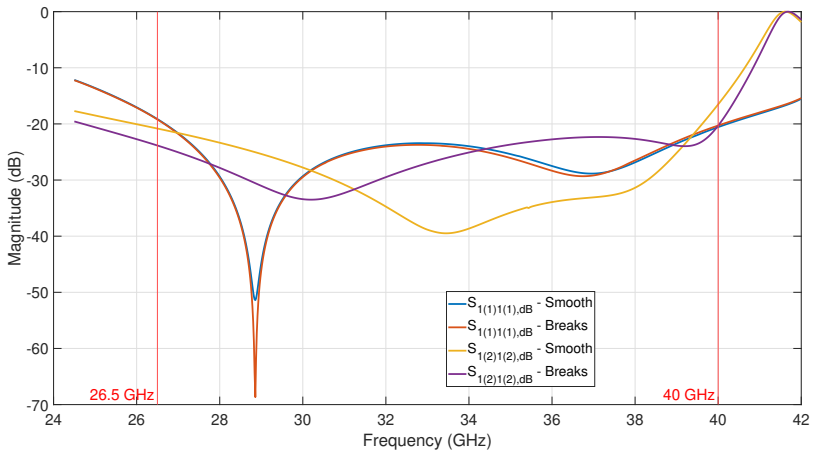

(a):

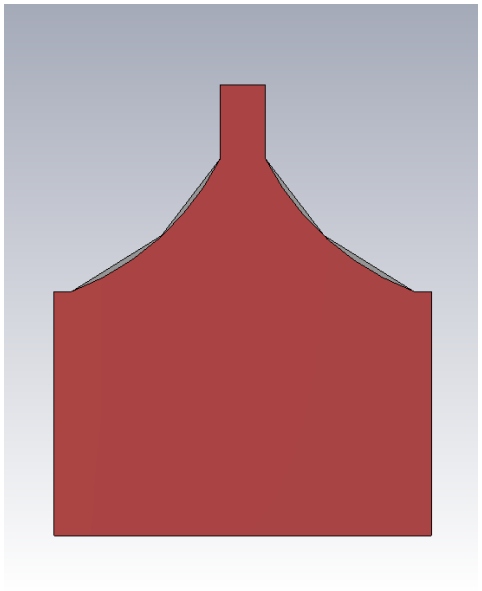

(b):

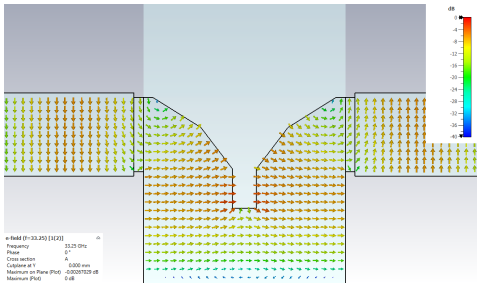

(c):

Figure 10: a) Parameters for both septum shapes, b) Septum shapes, c) E field of TE_{01} in septum region

Axial port transformer

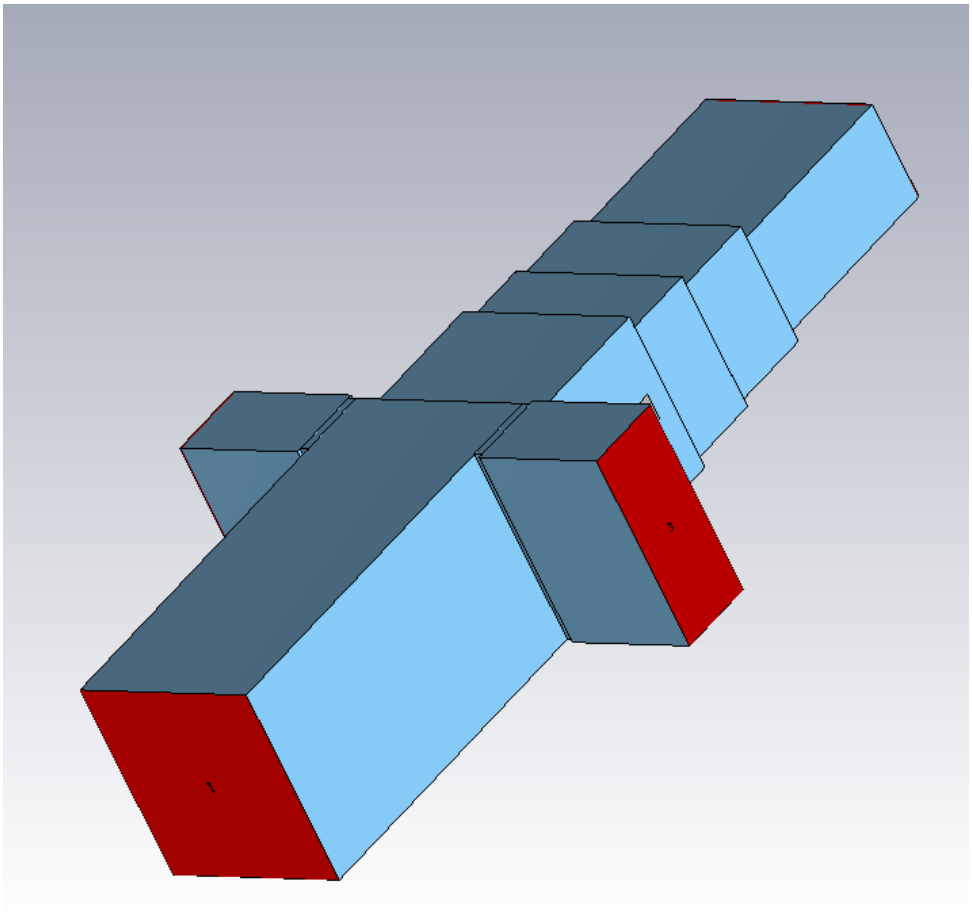

Figure 11: OMT base with axial port transformer

The next step was to design transformer for the axial port, that would lower the height of it to the WR28 output waveguide final dimensions. For this, synthesis tool of Fest3D was used, that quickly synthesises the required transformer according to input parameters. In [1], an algorithm for calculating the transformer dimensions can also be found, which also outputs transformer widths, in case the input and output widths are not equal. The transformer is symmetrical two-step and goes from the height of axial port, which is a little less than that of common waveguide, to output waveguide height, which is half of the common waveguide. Because the common waveguide width is same as output waveguide width, transformer only needs to transform the height dimension. As can be see in figure 12.a, the transformer only really affects the TE_{10} (1) mode, of which the return loss $S_{1(1)1(1)}$ has changed. Other parameters like transfer between single mode ports have not changed considerably during this phase and still remain around the same level. The transformer was designed so that the return loss is below $-20\,\mathrm{dB}$, as shown in figures 12.a and 12.c. At this stage, some resonance could be seen at certain

frequencies. This was because some energy of mode TE_{01} got past the septum region at these frequencies, but could not continue pass the transformer due to its narrowing and got stuck between the transformer and septum. This was easily solved by making the septum longer, which attenuated this mode more at these frequencies.

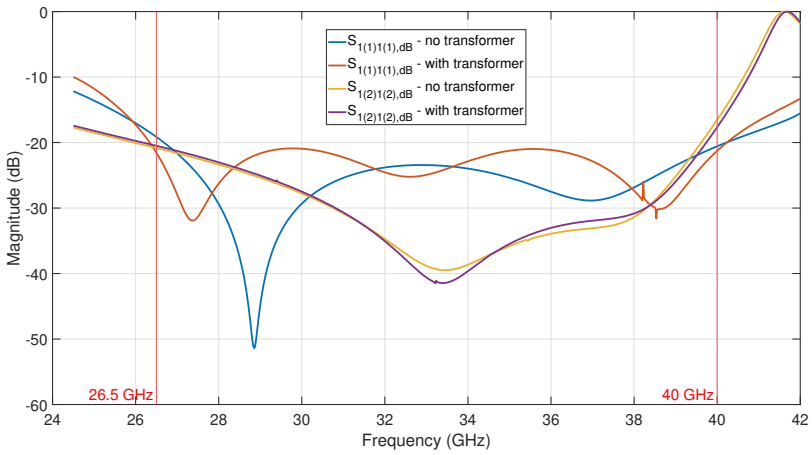

(a):

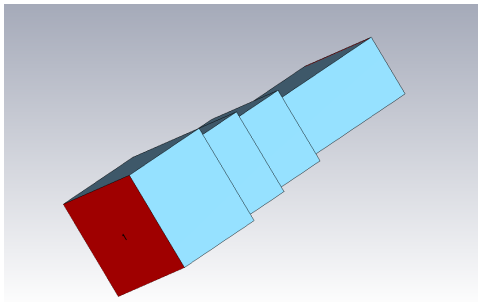

(b):

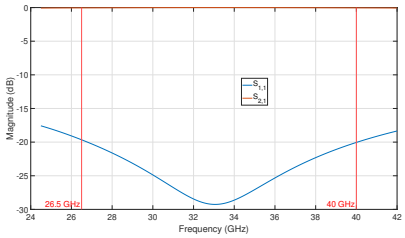

(c):

Figure 12: a) Tuned parameters of the OMT base with axial port transformer, b) The axial port transformer, c) Parameters of standalone axial port transformer

Combining the side ports

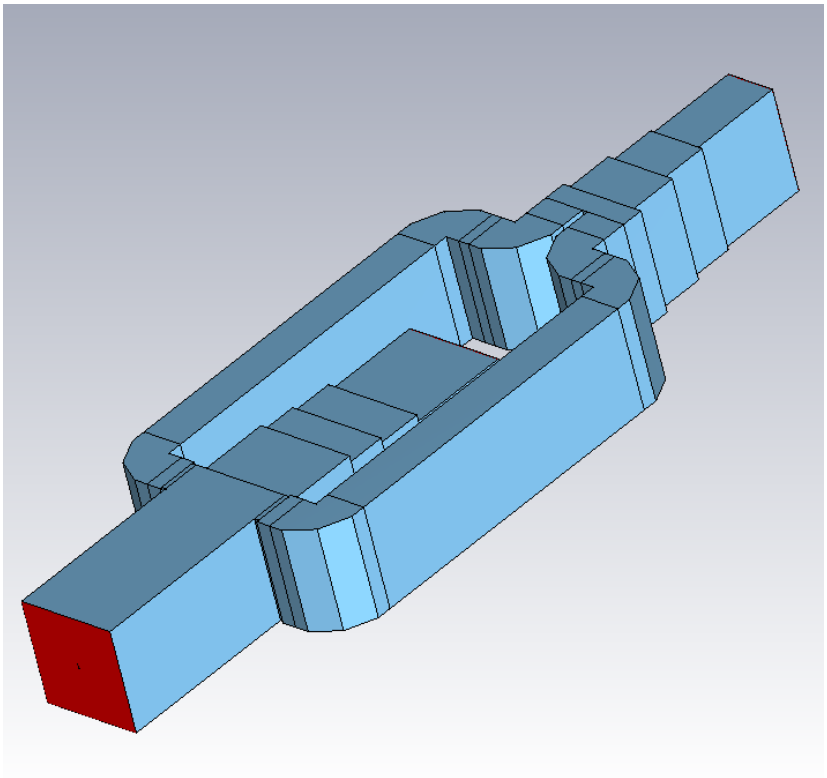

Figure 13: OMT with side ports power combiner/divider

The following step was to combine the side ports, which could be done by either using E plane bends or H plane bends, as discussed in the section about Bøifot junction. E plane bends were used here, since they are easier to manufacture, due to being in the same plane as the rest of the OMT so far and also because they offer bigger bandwidth. Designing how to combine these bends and also the power combiner took quite a bit of testing and thought. Firstly, only single mitred bends were tried in the design, but the return loss proved too big, so double mitred bends were used, as seen in figure 14.b, which cause very little return loss. Than the combiner was designed with the help of [1]. Basically, the sidearm branches connect to a common waveguide, separated through a thin septum, as in figure 14.f. That is followed by a two step transformer, which transforms this common waveguide into WR28 output waveguide. Again, because we used square input waveguide that has the same dimension as the width of the output waveguide, there is no need to transform the waveguide width anywhere alongside the path of the signal and only the height needs to be transformed. This whole assembly of bends, branches and combiners had very little effect on the TE_{10} (1) mode, as expected, and only effects the return loss $S_{1(2)1(2)}$ of TE_{01} (2) mode, as shown in figure 14.a.

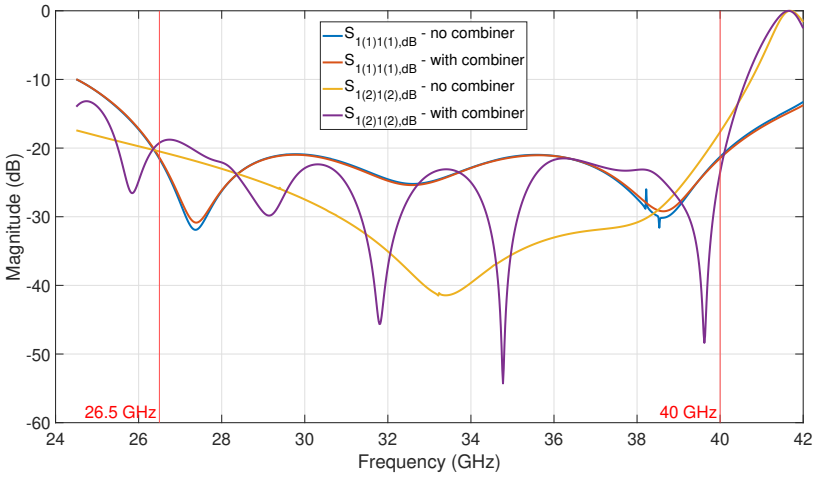

(a):

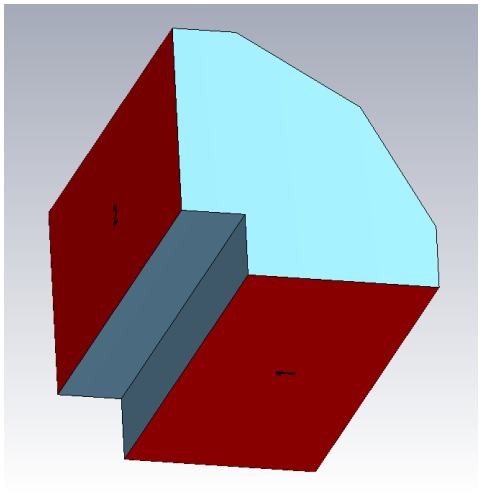

(b):

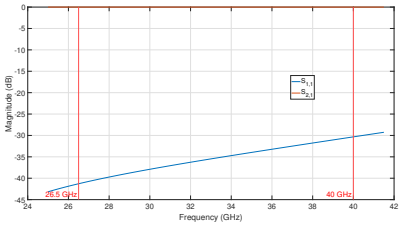

(c):

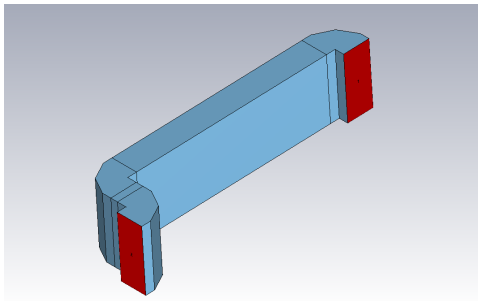

(d):

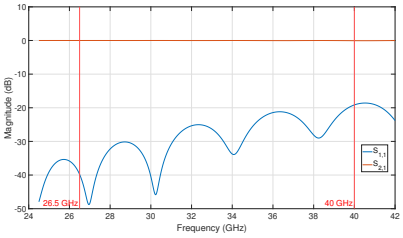

(e):

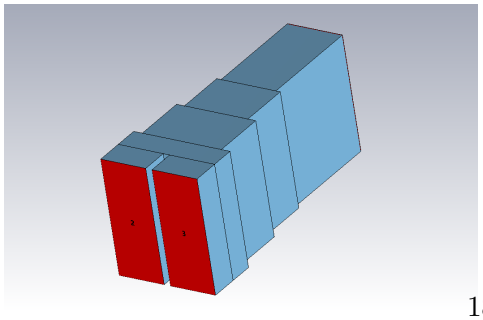

(f):

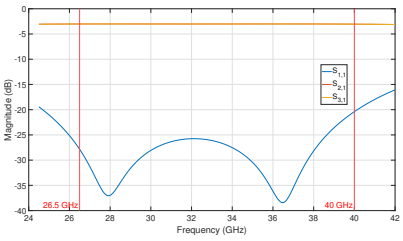

(g):

Figure 14: a) Tuned parameters of the OMT with side ports connected, b) Bend used in the side port waveguide branch, c) Parameters of standalone bend, d) Side port branch, e) Parameters of standalone branch, f) Power combiner for side port branches, g) Parameters of standalone power combiner

Axial port output

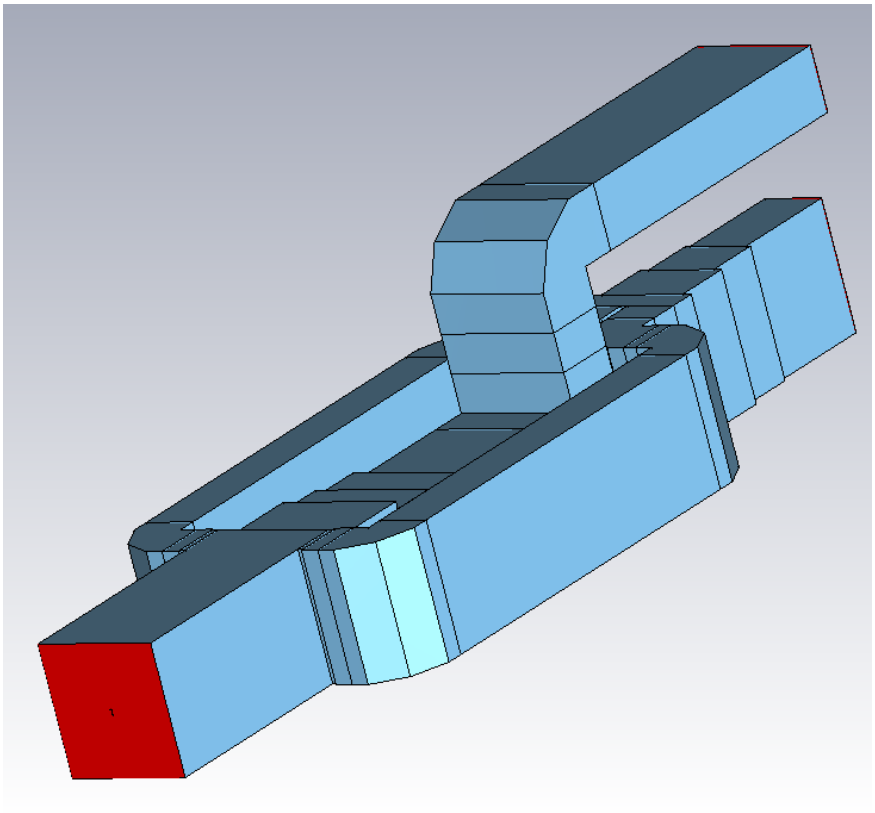

Figure 15: OMT with sharp edges and corners

One of the last steps in the OMT design is to design the axial port output. This output is often done by making a 90° bend at the place of the axial transformer output, and is then brought to the side, as in [5]. During the design of this OMT, idea came up about designing it such that this output also comes out the back, as the sidearm output. The paths to both WR28 waveguides should ideally be the same electrical length across the whole frequency band. That way, circular polarization can be obtained by shifting one of the port signals by 90°. This has led to solution showed in figure 16.d. This output branch consists of two 90° bends, a short waveguide connecting these two bends and a waveguide that brings the output to the same plane as the side port output. The bend design was very similar to the design of bends in the side branches, difference being that the waveguide now has WR28 dimensions. The axial port branch, shown in figure 16.d, has very low return loss and doesn't effect the TE_{10} (1) mode much, also has no effect on TE_{01} (2) mode. The structure was optimized, so that phases of $S_{2(1)1(1)}$ and $S_{3(1)1(2)}$ parameters are as similar as they can be.

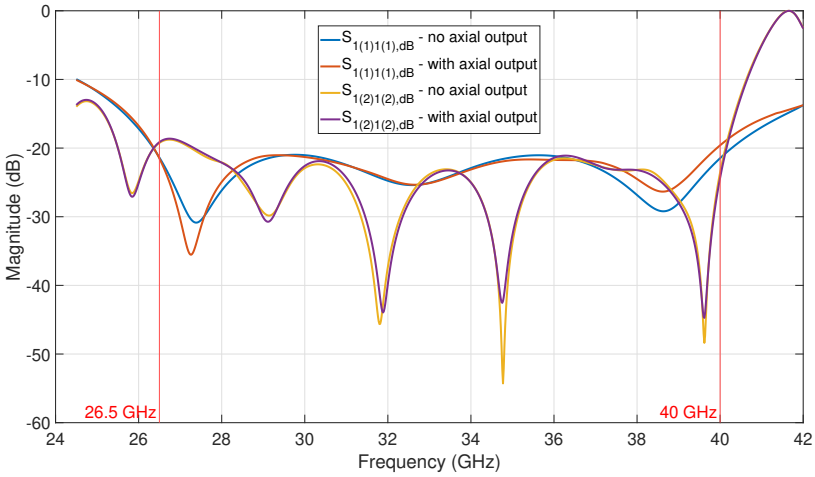

(a):

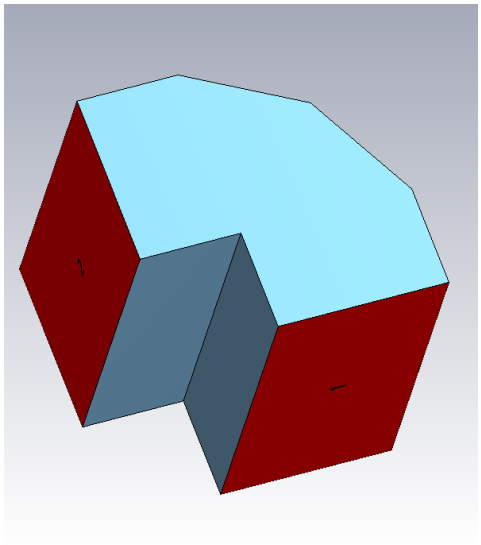

(b):

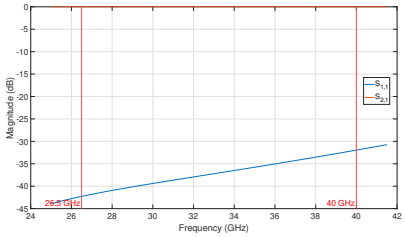

(c):

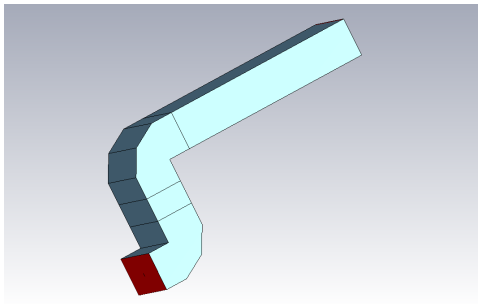

(d):

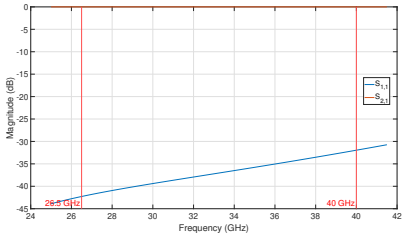

(e):

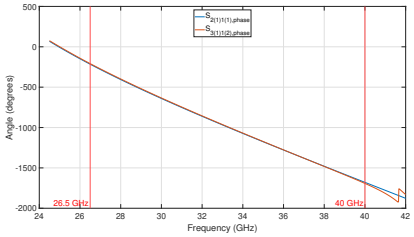

(f):

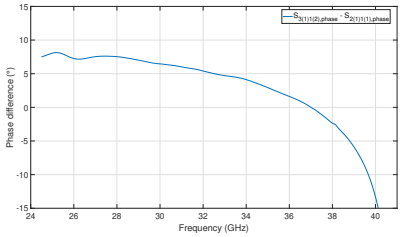

(g):

Figure 16: a) Tuned parameters of the OMT base with completed axial port output, b) Bend used in the axial port output branch, c) Parameters of standalone axial port bend, d) Axial port output branch, e) Parameters of standalone axial port output branch, f) Phases of $S_{2(1)1(1)}$ and $S_{3(1)1(2)}$ parameters, g) Phase difference

Blending the edges and corners

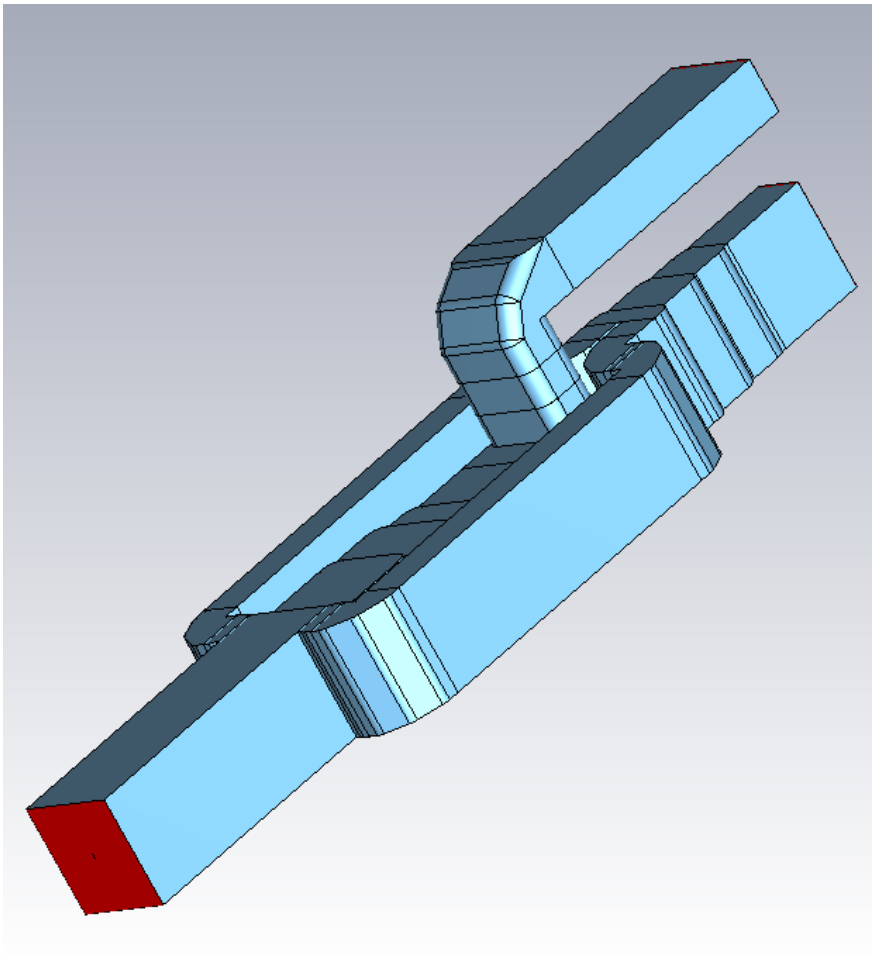

Figure 17: OMT with blended edges and corners

Last step of the standalone OMT design was to round the sharp edges and corners, that could not be machined, to get a more accurate model. After some testing, good results were obtained with radius $r = 1\,\text{mm}$, for all the edges and corners. This structure was highly optimised, to obtain low return loss at the ports and to get lowest possible phase difference of $S_{2(1)1(1)}$ and $S_{3(1)1(2)}$ parameters. The results at this stage got even better, than the previous stage, where edges and corners were left sharp. The septum at this stage is 0.914 mm thick, which should be easily scalable to the W frequency band, with all the other dimensions and the radius for edges and corners. One thing to note about this design is that the single mode input/outputs being quite close together, 9.44 mm, which does mean an special flange or some other way to connect to these ports would be needed, since standard UG599/U flange would not fit.

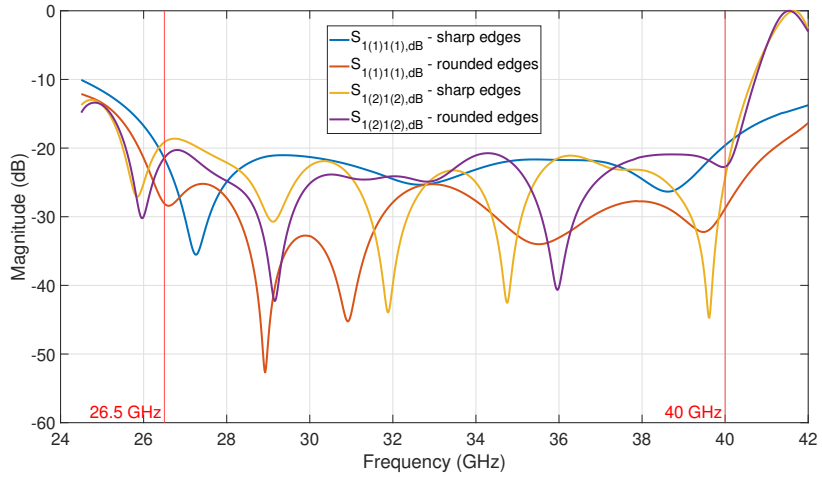

(a):

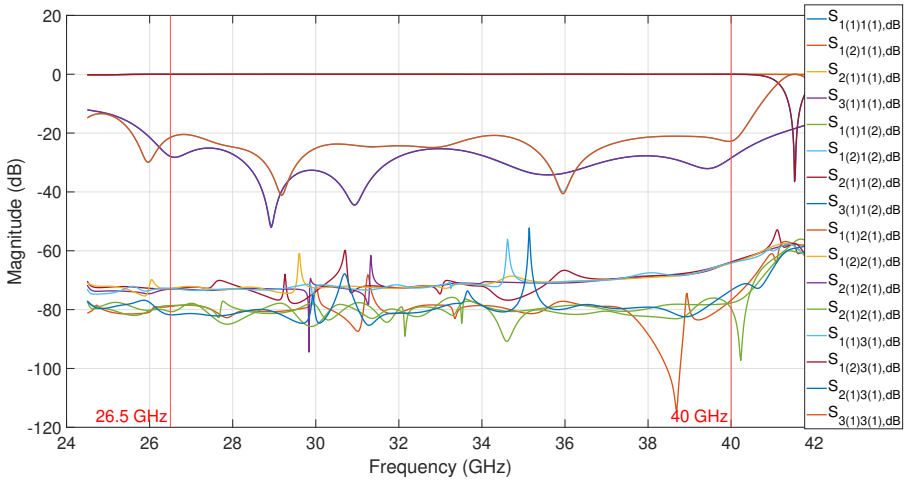

(b):

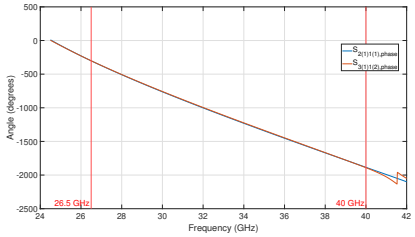

(c):

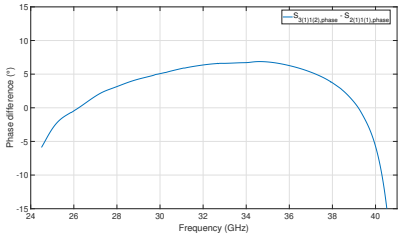

(d):

Figure 18: a) Difference in parameters of OMT with sharp and blended edges and corners, b) Tuned parameters of the OMT with blended edges and corners, c) Phases of $S_{2(1)1(1)}$ and $S_{3(1)1(2)}$ parameters of OMT with blended edges and corners, d) Phase difference of OMT with blended edges and corners

For further steps, the OMT model needed to be transformed from PEC background material with vacuum structures to vacuum background with PEC structures. This was done be changing the background type and encasing the whole structure in PEC block, from which the vacuum parts were subtracted, as shown in figures 20.a and 20.b. This transformation does not really effect the parameters, shown in figure 19, which is expected. It also increased number of cells and computation time.

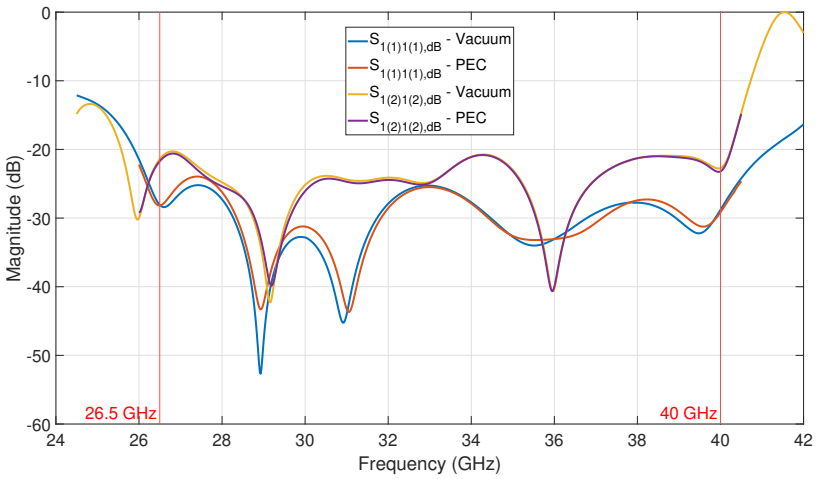

(a):

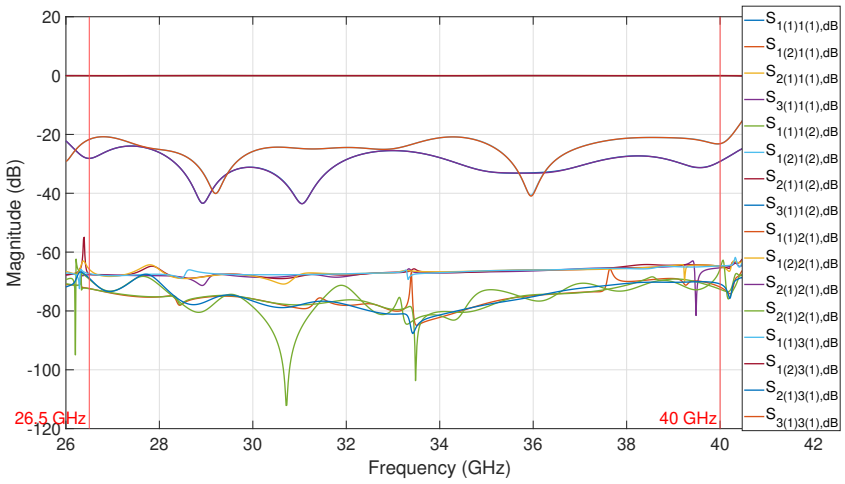

(b):

Figure 19: a) Difference in parameters between vacuum and PEC version of the OMT model, b) PEC OMT model

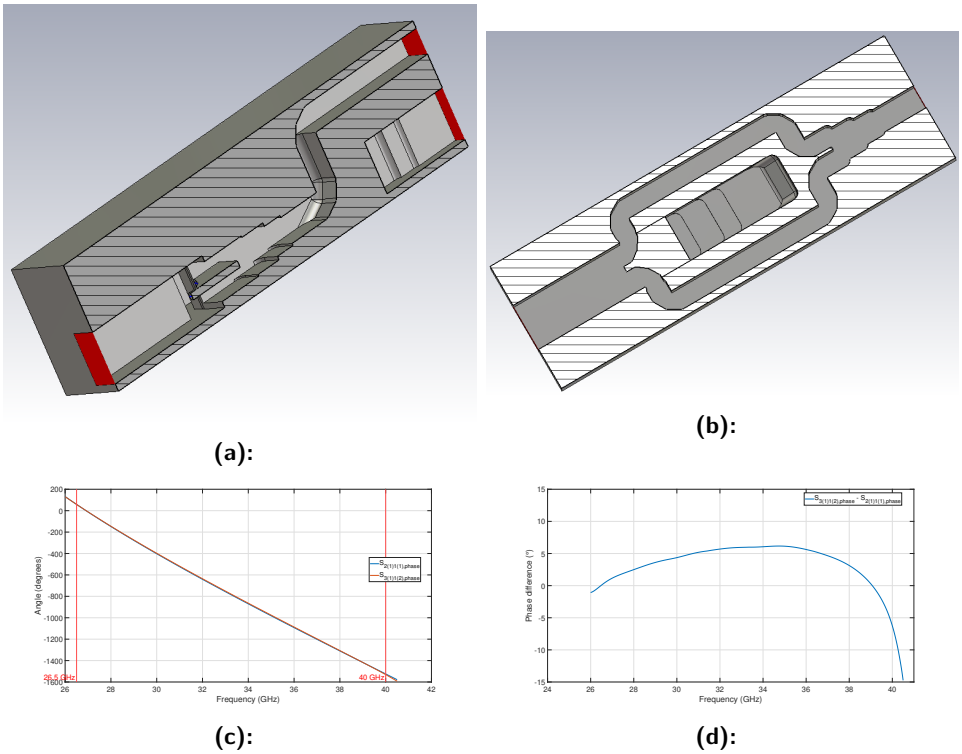

Figure 20: a) and b) PEC OMT model, c) Phases of $S_{2(1)1(1)}$ and $S_{3(1)1(2)}$ parameters of PEC OMT model, d) Phase difference of of PEC OMT model

Antenna

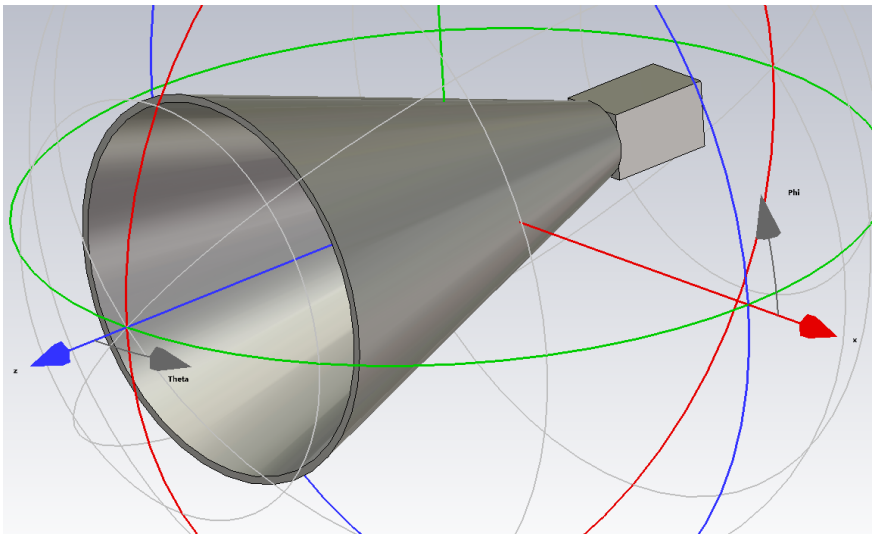

Figure 21: Conical horn antenna connected to square waveguide

After being done with the standalone OMT model, the final device also requires a horn antenna with gain of at least 20 dBi. Conical horn antenna was designed with the help of Antenna Magus, which is design software included in CST Studio Suite. The design of this antenna is pretty simple, it needs to be long enough and have big enough flare diameter to achieve the desired gain and bandwidth. The diameter of input, which connects to the square waveguide, that represents the OMT square common waveguide, needs to be such that return loss is as low as possible. Watched parameters when tuning this antenna are the return loss and also gain across the frequency band. The antenna should also be linearly polarised when excited with TE_{10} or TE_{01} mode, which is represented by axial ratio. In figure 22.a, it can be seen, that return loss is below -20 dB, the gain is above 20 dBi and axial ratio is 40 dB across the whole frequency band. The sidelobe level is -17 dB for the center frequency and is the worst at -15.5 dB at 40 GHz. The result are exactly the same for the TE_{01} mode, but the radiation patterns are switched, so that radiation pattern for $\phi = 0°$ for mode the same as radiation pattern $\phi = 90°$ of TE_{01} mode.

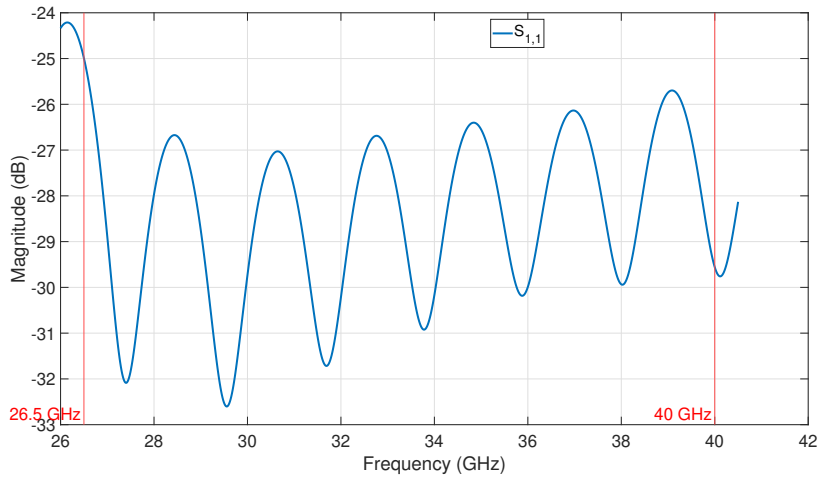

(a):

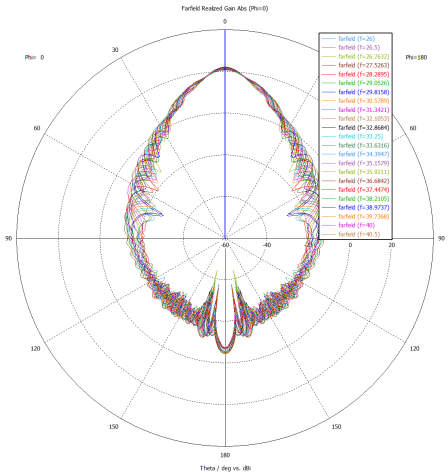

(b):

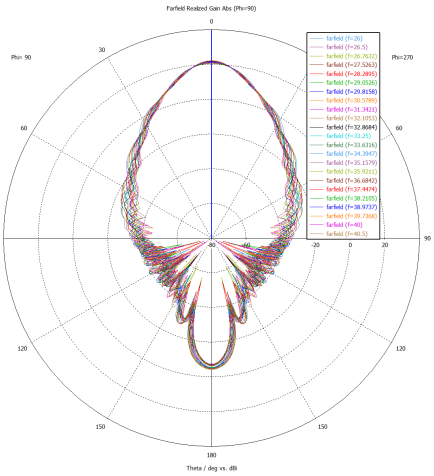

(c):

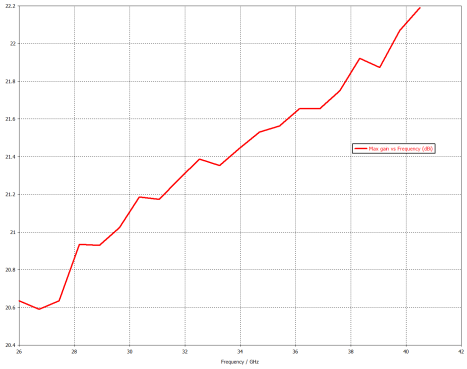

(d):

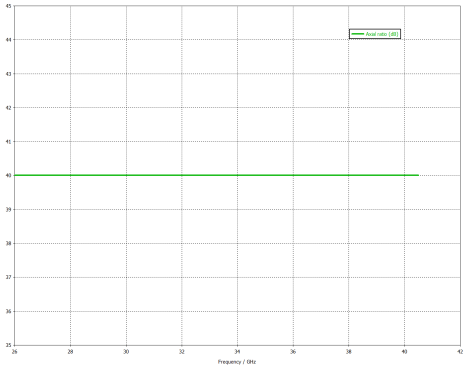

(e):

Figure 22: a) and b) Antenna radiation patterns for $\phi = 0°$ and $\phi = 90°$ for TE_{10} mode, c) Antenna maximum gain vs frequency ,d) Antenna axial ratio vs frequency

Adding the antenna to the OMT and scaling

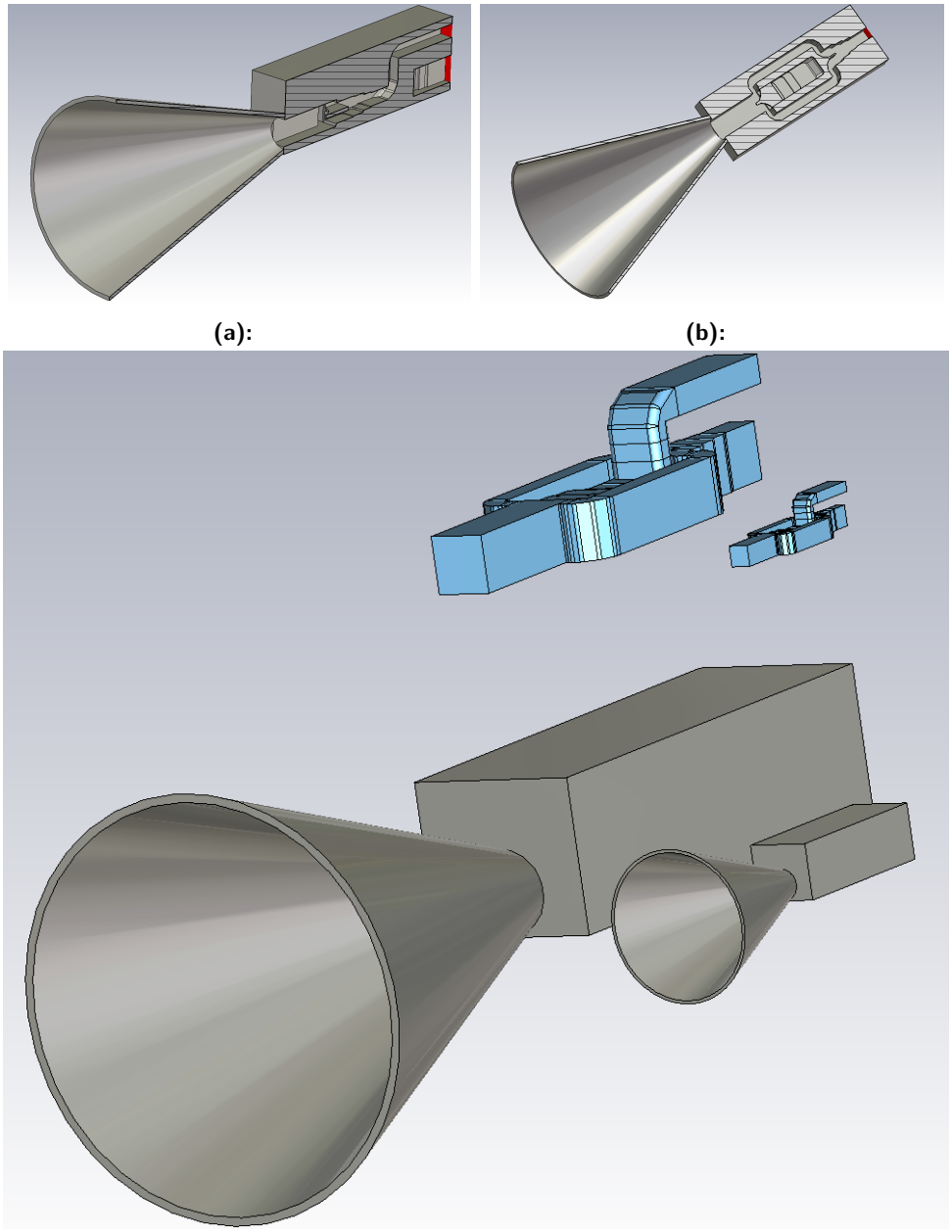

Figure 23: a) and b) Final design of the OMT with added antenna, c) Size comparison of Ka band a W band OMT designs

To complete the design, the antenna was added to the OMT. Now only single mode ports 2 and 3 remain, as the common waveguide is connected to the antenna. Connecting the antenna to the OMT changed the parameters quite a bit, with some peaks going above $-20\,\mathrm{dB}$ when looking at return losses,

as shown in figure 24.a. Nevertheless, the design still performs very well, the transfer between ports 2 and 3 is still very low and gain and axial ratio remain almost unchanged. The radiation patterns, gain and axial ratio are very similar to standalone antenna from previous step, figure 25. Overall, this design achieves set goals and shows promising results. Complete dimensions of the OMT are in the appendix.

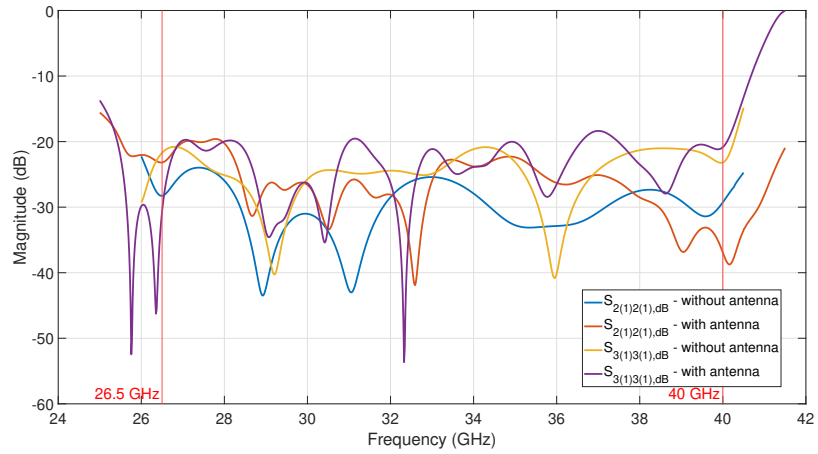

(a):

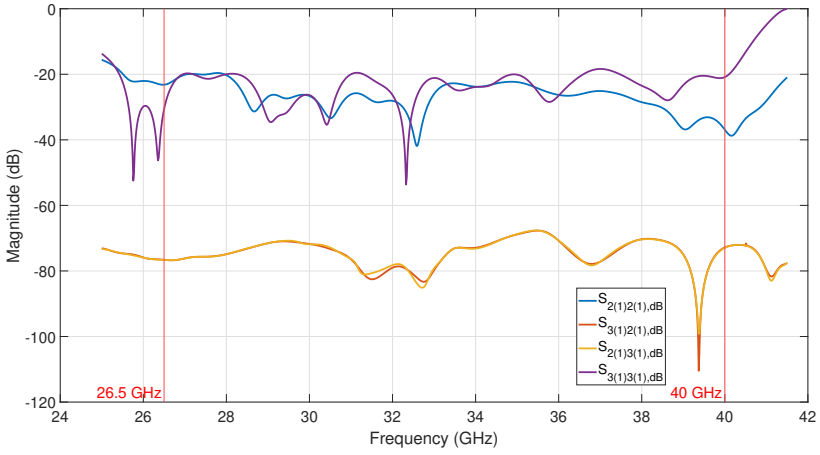

(b):

Figure 24: a) Difference in parameters between OMT PEC model and OMT model with antenna, b) Parameters of OMT with antenna

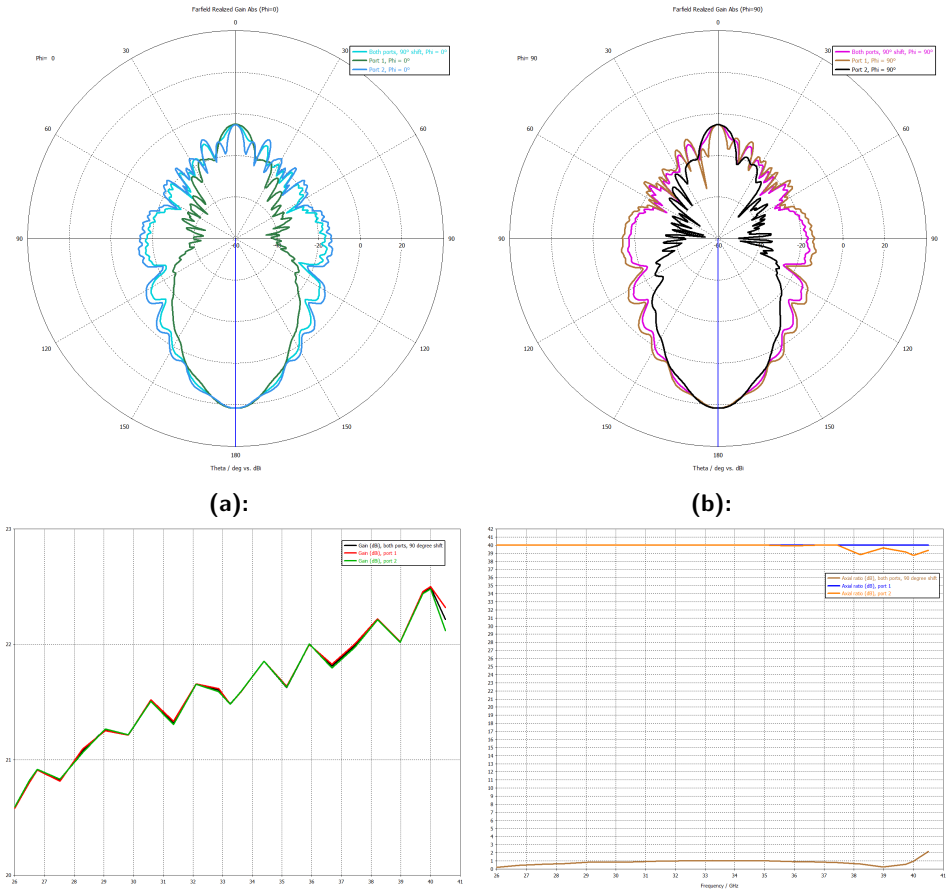

(a): **(b):**

(c): **(d):**

Figure 25: a) and b) OMT with antenna radiation patterns for $\phi = 0°$ and $\phi = 90°$ at centre frequency for single port excitation and simultaneous port excitation, c) OMT with antenna maximum gain vs frequency d) OMT with antenna axial ratio vs frequency

The only thing left to complete the design of the W band was to scale this design to fit WR10 waveguides and see if it functions as it should at these higher frequencies, as explained at the start of this chapter. CST MS allows to scale models, so this step was very easy to do. The W band model is roughly one third the size of the Ka band model, as expected. The scale worked very well and this design achieves very similar parameter as the Ka band OMT model. The bands differ slightly, because the scaling factor used comes from WR28 and WR10 width ratio, if scaling factor came from center frequencies of these bands instead, parameters in these bands would look the same.

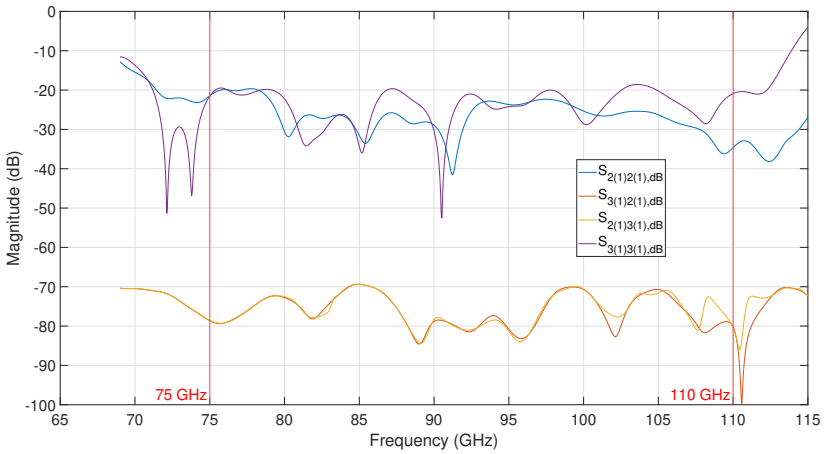

(a):

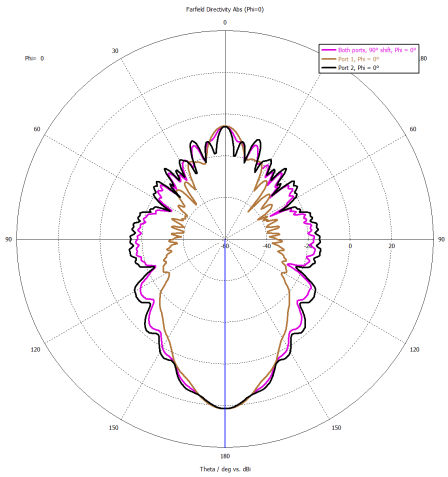

(b):

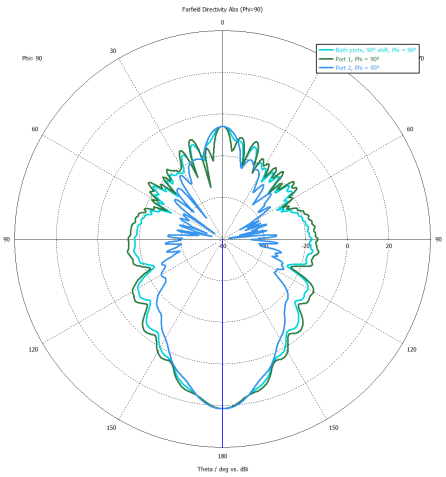

(c):

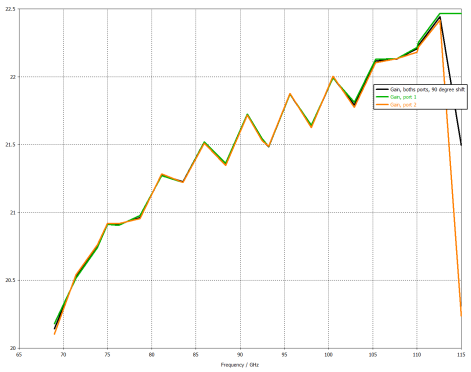

(d):

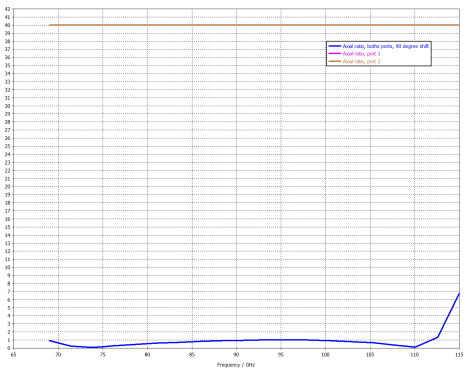

(e):

Figure 26: a) W band OMT model parameters, b) and c) W band OMT radiation patters for $\phi = 0°$ and $\phi = 90°$ at centre frequency for single port excitation and simultaneous port excitation, d) W band OMT maximum gain vs frequency, e) W band OMT axial ratio vs frequency

Measuring the OMT performance

The OMT for Ka band was manufactured for measuring and testing. Before that, coaxial probes were added to the model to make this easier. Model for these probes were provided externally by Ing. Zdeněk Hradecký Ph.D from RF Spin.

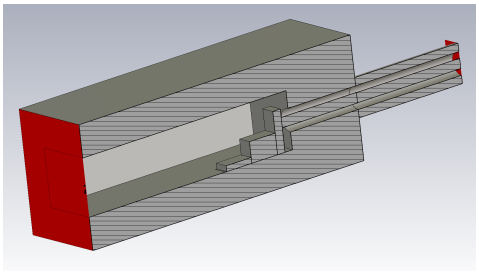

(a):

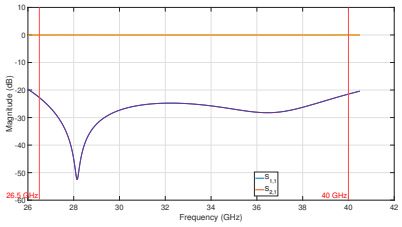

(b):

Figure 27: a) Coaxial probe, b) Coaxial probe parameters

Adding these probes affected the model parameters a little, mainly the return losses, while other parameters were not affected too much. The model still remains functional, and was being manufactured for about 1 month.

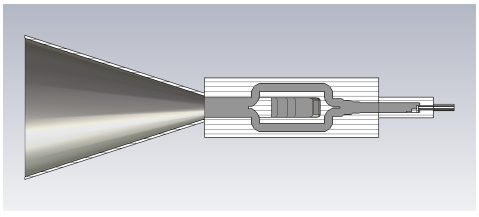

(a):

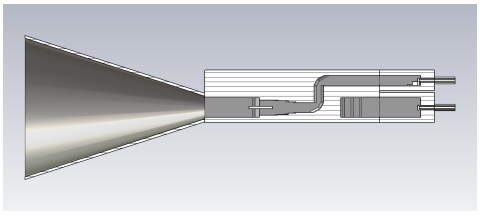

(b):

Figure 28: a) and b) OMT model with coaxial probes

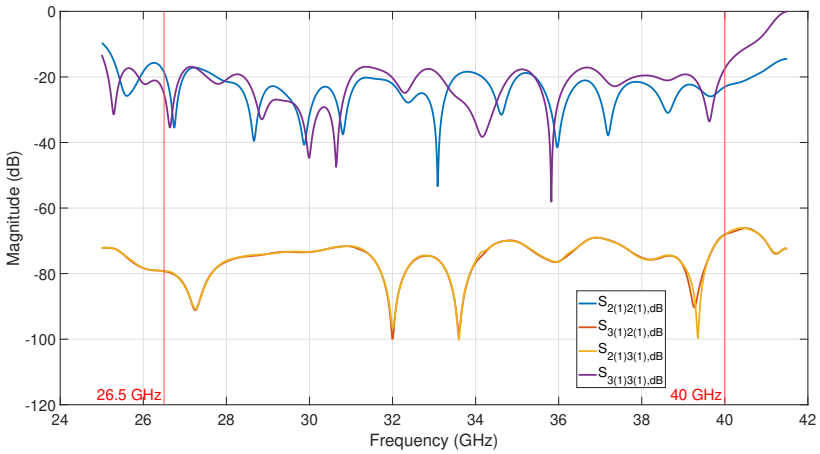

(a):

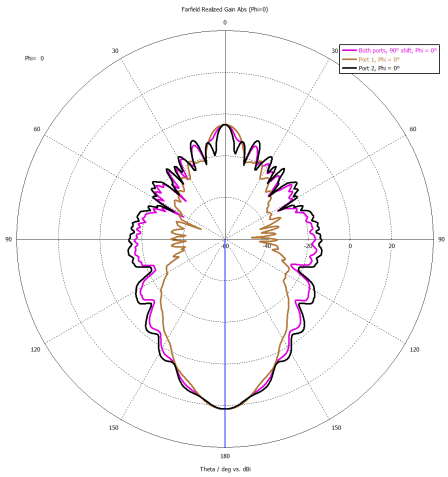

(b):

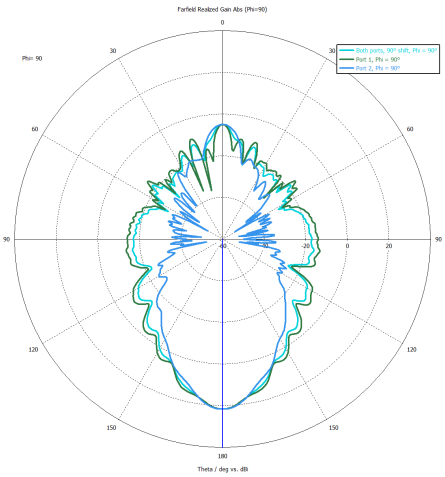

(c):

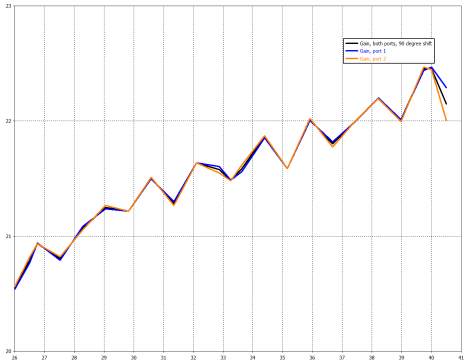

(d):

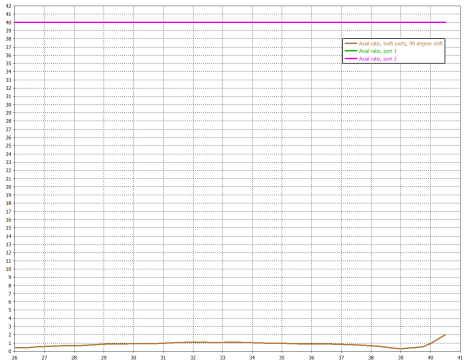

(e):

Figure 29: a) Difference between OMT models with and without connectors, b) Parameters of OMT model with connector, c) OMT with connectors radiation patters for $\phi = 0°$ and $\phi = 90°$ at centre frequency for single port excitation and simultaneous port excitation c) OMT with connectors maximum gain vs frequency f) OMT with connectors axial ratio vs frequency

After being manufactured, the OMT was measured at CTU Antenna laboratory. Two pieces of the OMT were manufactured, so any differences between them could also be measured. Cited from CTU website, the antenna laboratory has following parametrs.

> This lab is constructed as a Full Anechoic Chamber (FAC) with special measurement equipment for performing basic antenna parameters measurements (input impedance, WSVR, radiation pattern, polarization, gain) and measurements of radiated emissions in the field of EMC testing.
>
> *Antenna parameters measurements:*
> Operational frequency range: 200 MHz – 40 GHz (up to 110 GHz using the frequency extenders)
> Test ranges: 1 m – 4.5 m
>
> *EMC measurements:*
> Operational frequency range: 30 MHz – 3.3 GHz
> Test ranges: 1 m – 3 m
>
> *Measurement equipment:*
> Far-field Antenna Measurement System NSI 800F-30
> Vector network analyzer Rohde & Schwarz ZVA40,
> Test receiver Rohde & Schwarz ESRP
> Anritsu Sitemaster S400A and S820
> Broadband/narrowband antennas (200 MHz to 110 GHz)

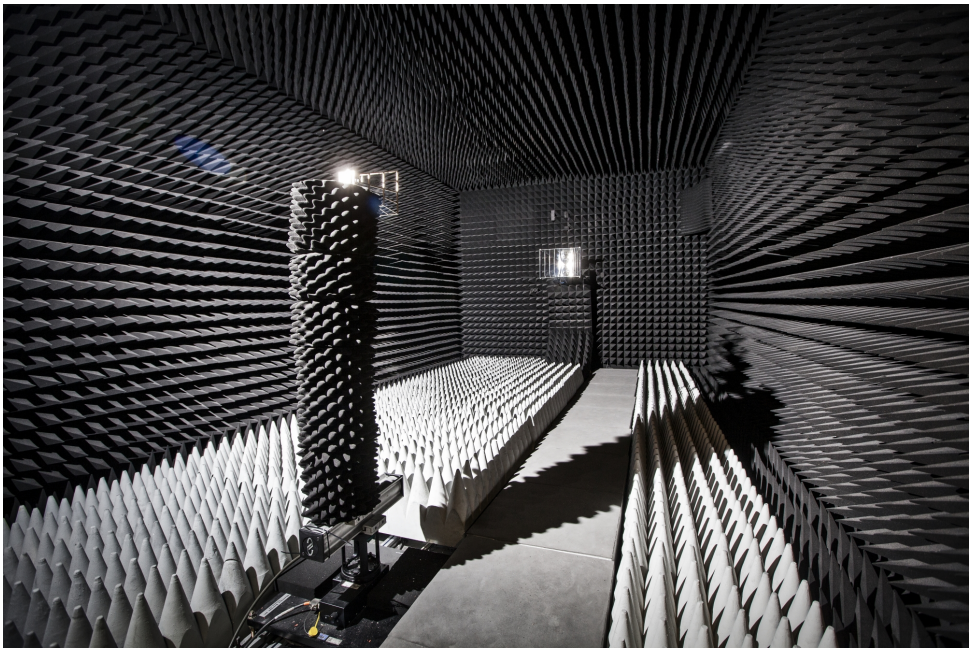

Figure 30: CTU antenna laboratory

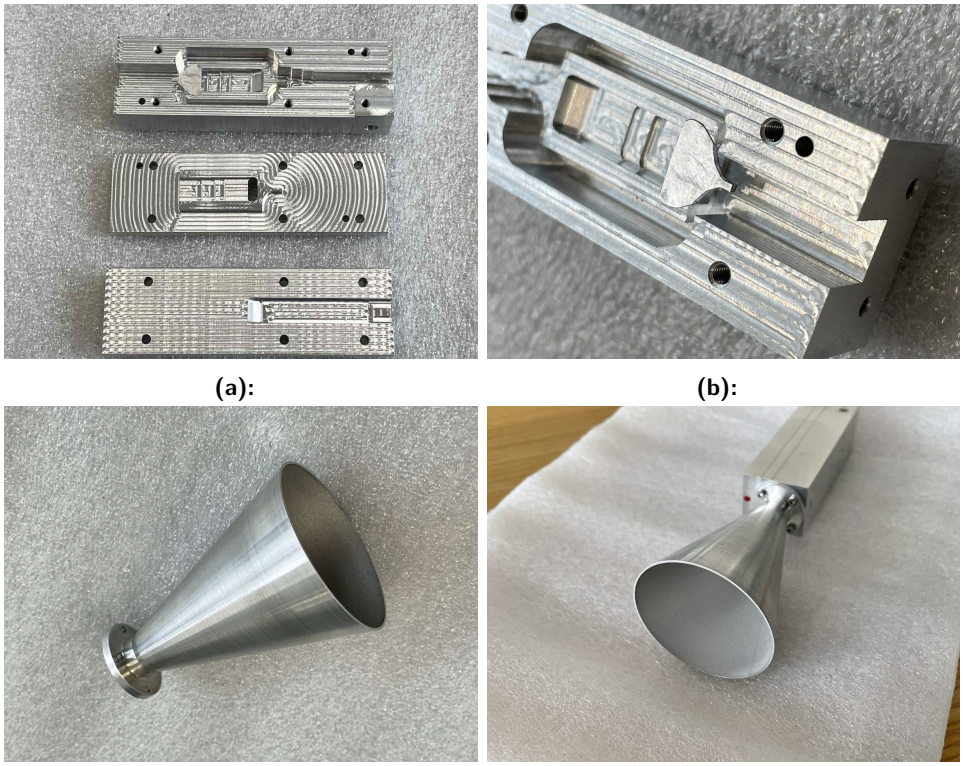

(a): **(b):**

(c): **(d):**

Figure 31: Manufactured OMT with conical horn antenna

Measurements

Several parameters were measured. This includes s-parameters, gain, polarization clarity, radiation patterns and axial ratios.

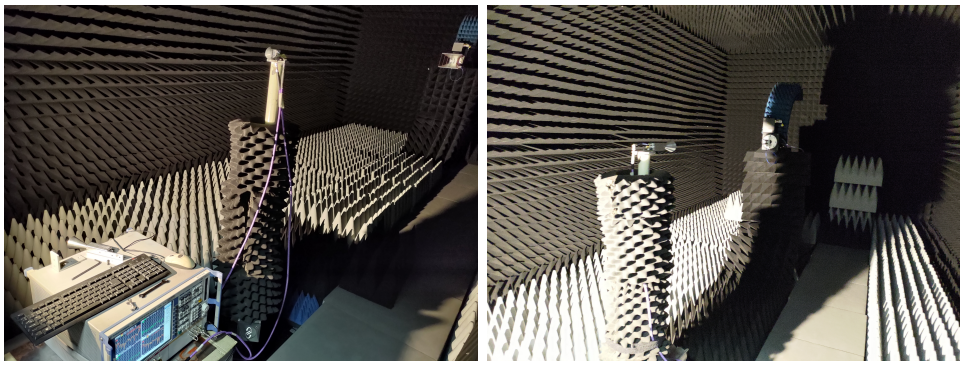

(a): **(b):**

Figure 32: a) S parameters measurement, b) Polarization and radiation pattern measurement

S-parameters

S-parameters of both OMTs were measured using vector analyzer in the antenna lab. The setup can be seen in figure **??**.a. The results show the manufacturing was very consistent and that OMT works reasonably well in the Ka frequency band, although the measured results are worse than expected. Some peaks reach almost $-10\,\mathrm{dB}$ for the return loss parameters, which is not a great performance. Transfer between ports is very low at around $-50\,\mathrm{dB}$ to $-60\,\mathrm{dB}$, which is a great result.

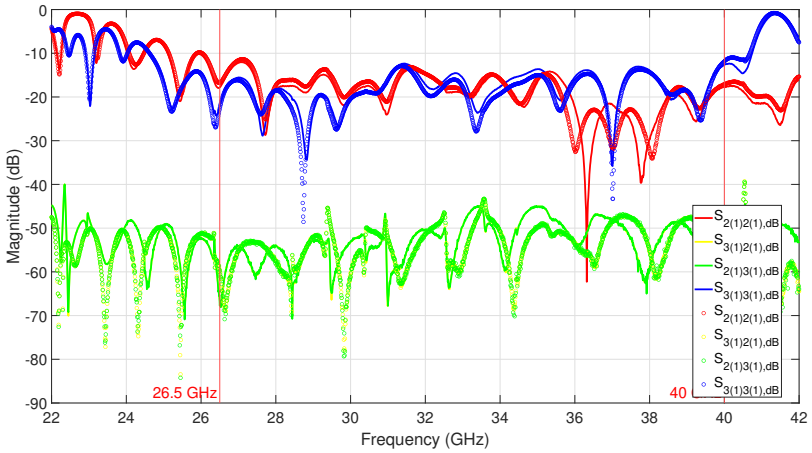

Figure 33: Measured s-parameters of two OMT devices

The reason why

Gain

Gain was measured using both OMT devices and Friis transmission formula to calculate the average gain of the two devices, which presumably is very similar. By connecting one port of each OMT device to the vector analyzer and terminating the other port, we were able to obtain 4 sets of port combinations. From these, we can calculate the average gain for both ports and also get some idea about cross-polarization discrimination. By modifying the Friis transmission formula, we get the following equation

$$G_{2/3} = \frac{S_{21;22/33} + FSL}{2}. \tag{4}$$

$G_{2/3}$ is the average gain of the OMT devices when exciting either the port 2 or port 3, $S_{21;22/33}$ is the measured transmission exciting either the port 2 or port 3 and also receiving on the same port on the second device, FSL is free space loss. All units are in dB, except gain, which is in dBi. Free space loss can be calculated using following formula

$$FSL = 20\log\left(\frac{4\pi}{c} l f\right), \tag{5}$$

where c is the speed of light in vacuum/air, l is distance between apertures and f is frequency. Apertures were 1 m apart when doing this measurement, which is more than antenna far field zone, calculated like

$$l_{farfield} \geq \frac{2D^2}{\lambda}, \tag{6}$$

where D is the diameter of the horn antenna and λ is wavelength of the highest frequency we want to measure. Since our horn antenna has a diameter of approximately 5 cm, far filed zone for frequency of 40 GHz is approximately 0.7 m. Using these equations we get the averaged gains for both port excitations, shown in figure 34. The calculated gains are very similar to our simulated results.

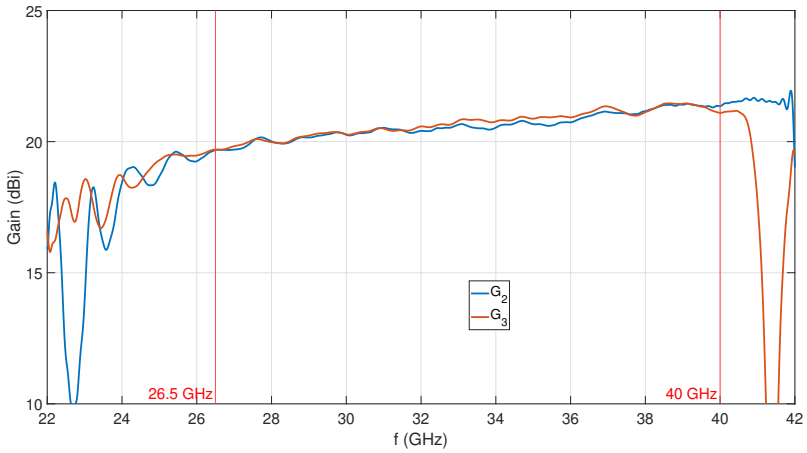

Figure 34: Calculated gains G_2 and $G3$

Since we now know these gains, we can get some idea about cross-polarization discrimination of the OMT devices, using transfer parameters where different port is used on each device. We can put L_{x-pol}, losses due to cross-polarization, into the Friss equation and get the following formula

$$L_{x-pol;23/32} = G_2 + G_3 - FSL - S_{12;23/32}. \tag{7}$$

The cross-polarization losses are around -40 dB to -50 dB, shown in figure 35, which indicates very good cross-polarization discrimination.

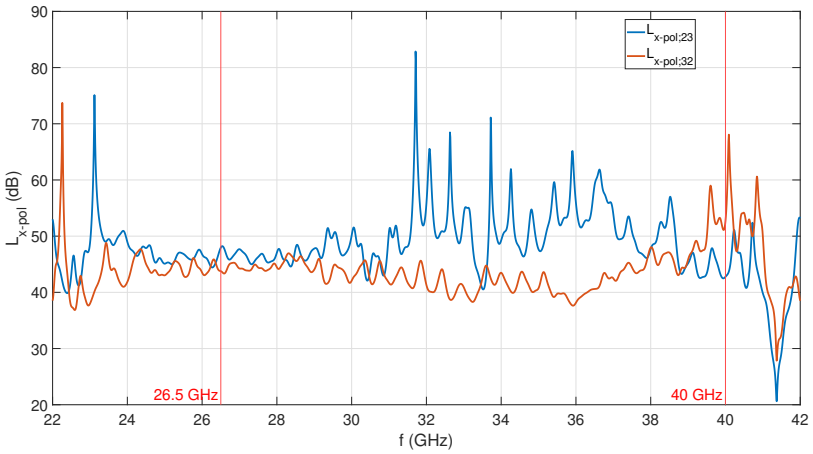

Figure 35: Calculated losses $L_{x-pol;23}$ and $L_{x-pol;32}$

Polarization clarity

Next measured parameter was polarization clarity, setup is shown in figure 32.b. The OMT is aimed at very linear horn antenna, which can rotate around its axis and change the polarization its receiving. This measurement was done with only one of the two OMT devices, where one port was connected to the vector analyzer, as well as the horn antenna and the second port was terminated. Measurement was done across the whole frequency range, from 22 GHz to 40 GHz and was normalized to maximum gain, shown in figure 36. Both figures show very large cross-polarization discrimination and basically confirm our presumptions from the gain measurement.

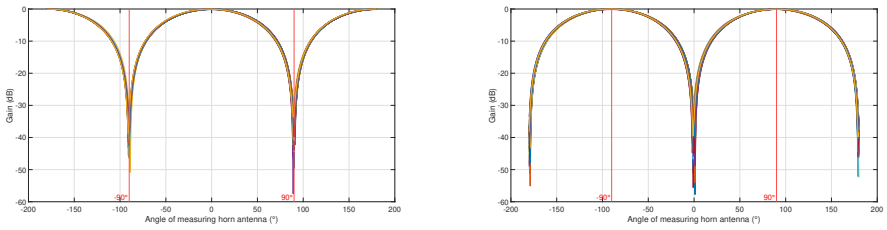

(a): **(b):**

Figure 36: a) Polarization measurement for port 2 excitement, b) Polarization measurement for port 3 excitement

Radiation patterns

Setup to measure radiation patterns was similar to the case of polarization clarity measurement, but this time the OMT device was rotating. 8 measurements were obtained, two ports, two radiation planes and also two polarizations, which means we also measured the cross-polarizations from which axial ratio can be extracted. Radiation patterns are very similar to those, that were simulated. $\phi = 0°$ co responds to the horizontal plane while $\phi = 90°$ corresponds to vertical plane.

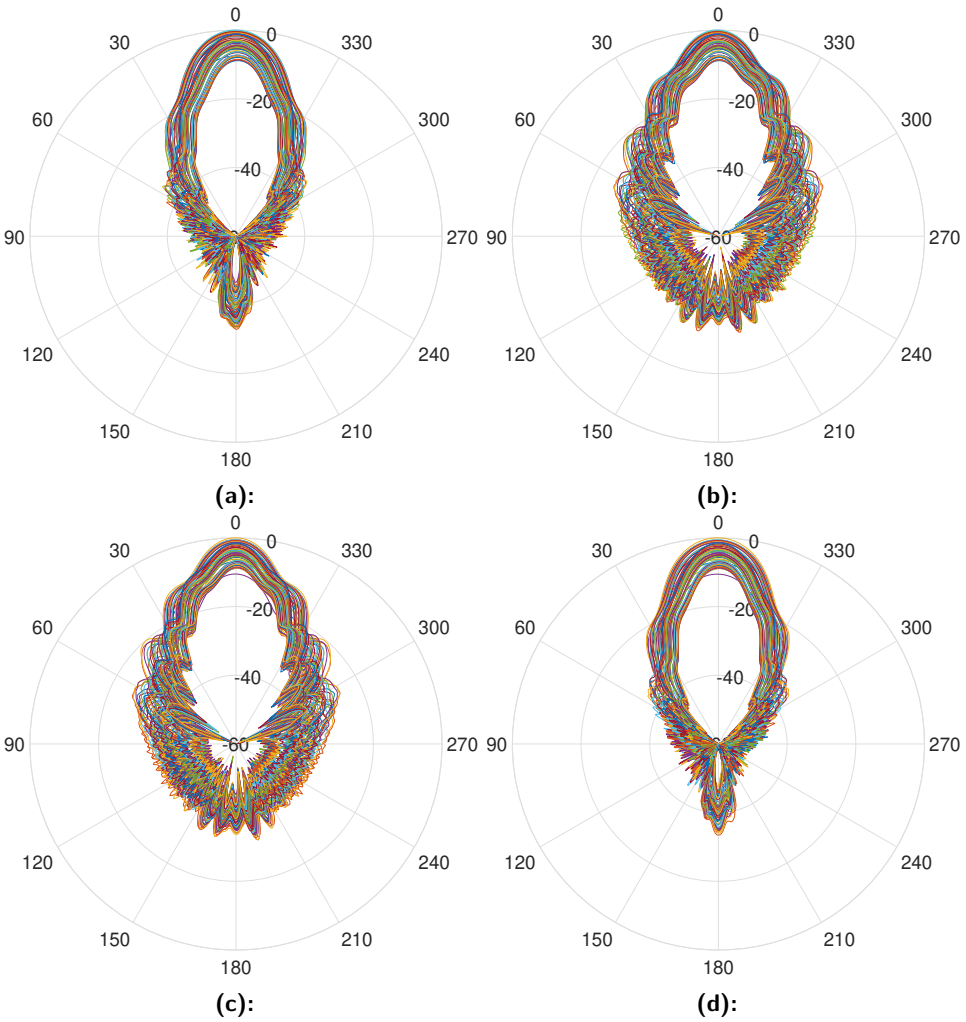

Figure 37: a) and b) Radiation patters for $\phi = 0°$ and $\phi = 90°$ for port 2, c) and d) Radiation patters for $\phi = 0°$ and $\phi = 90°$ for port 3

Axial ratio

Axial ratio was also calculated from polarisation data in the direction of largest gain direction, same as in simulations. Since two radiation planes were obtained for each port, there are also two ways to calculate the axial ratio, once from each plane. Even though they are not the same, which they theoretically should be, they are very similar and both axial ratios obtained for both ports are around 40 dB, which means the polarization is very linear and very close to simulated values and our previous calculations.

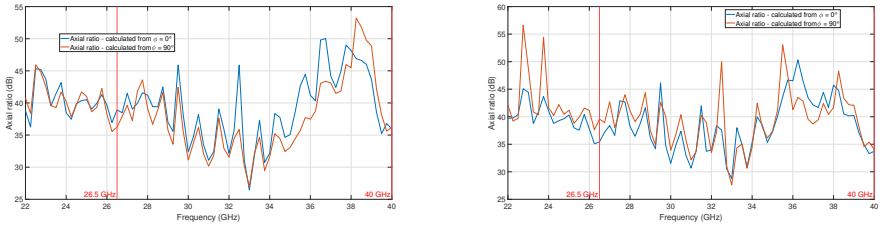

(a): **(b):**

Figure 38: a) Axial ratios for port 2 excitation, b) Axial ratios for port 3 excitation.

Conclusion

At the beginning of this thesis, concept and motivation for orthomode transducers were explained. Various types of narrowband and wideband OMT types were described. Advantages and disadvantages of these types were covered, with narrowband designs usually being easier to construct and design, while broadband designs offer bandwidth where its needed. One such orthomode transducer was than designed in CST Microwave Studio, together with an antenna, for Ka frequency band. The goal was to make the design scalable to W frequency. The ports were positioned such, that the electric path lengths for corresponding modes between common waveguide and single mode waveguide ports are as similar as possible, which was simulated, and allows for circular polarization by shifting one of the input signals by 90°. Design of this device was described step by step, with optimizing in between these steps to achieve the best results possible. The scaled version for higher W frequency band works very similar. Two of these devices devices were manufactured and measured in CTU Antenna Lab. Parameters were measured and compared to those obtained from simulation, with some being very similar like radiation patterns, gain and axial ration, while return loss parameters were measured worse than simulated. At this point, no reason for this change has been found, some more optimizations of the device could be made to improve these parameters.

Bibliography

[1] Uher, J., Bornemann, J. and Rosenberg, U., 1993. "Waveguide components for antenna feed systems: Theory and CAD". Artech House Antenna Library.

[2] Bøifot, A.M., 1991, "Classification of Ortho-mode transducers". Eur. Trans. Telecomm., 2: 503-510.

[3] A. Navarrini and R. L. Plambeck, "A turnstile junction waveguide orthomode transducer," in IEEE Transactions on Microwave Theory and Techniques, vol. 54, no. 1, pp. 272-277, Jan. 2006, doi: 10.1109/TMTT.2005.860505.

[4] R. Banham, G. Valsecchi, L. Lucci, G. Pelosi, S. Selleri, V. Natale, R. Nesti, and G. Tofani, "Electroformed front-end at 100 GHz for radio-astronomical applications," Microwave Journal, vol. 48, nº. 8, pp. 112-122 2005.

[5] Gopal N. and Neal R. Erickson "A Novel Full Waveguide Band Orthomode Transducer", Thirteenth International Symposium on Space Terahertz Technology, Harvard University, March 2002.

[6] E.J. Wollack, W. Grammer, and J. Kingsley, "The Boifot Orthomode Junction," , vol. 425 2002.

[7] Ignacio Izquierdo Martinez, "Design of wideband orthomode transducers based on the turnstile junction for satellite communications", Proyecto Fin de Carrera, Universidad Autónoma de Madrid, Nov. 2008.

[8] J. A. Ruiz-Cruz, J. R. Montejo-Garai, J. M. Rebollar, "Full-Wave Modeling and Optimization of Bøifot Junction Ortho-Mode Transducers", Int. J. RF Microw. Comput.-Aided Eng., 18, 4, pp. 303-313, June 2008.

[9] S.J. Skinner, and G.L. James, "Wide-band orthomode transducers," IEEE Transactions on Microwave Theory and Techniques, vol. 39, nº. 2, pp. 294-300, Feb 1991.

Ka frequency OMT band dimensions

All the dimensions are in mm. All blended edges are blended with a radius $r = 1\,\text{mm}$.

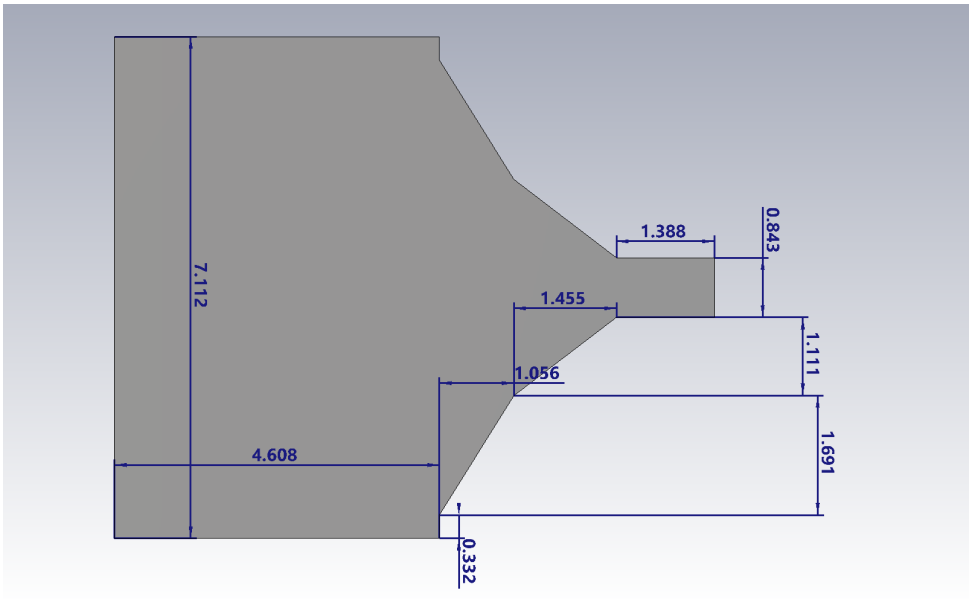

Figure 39: Septum

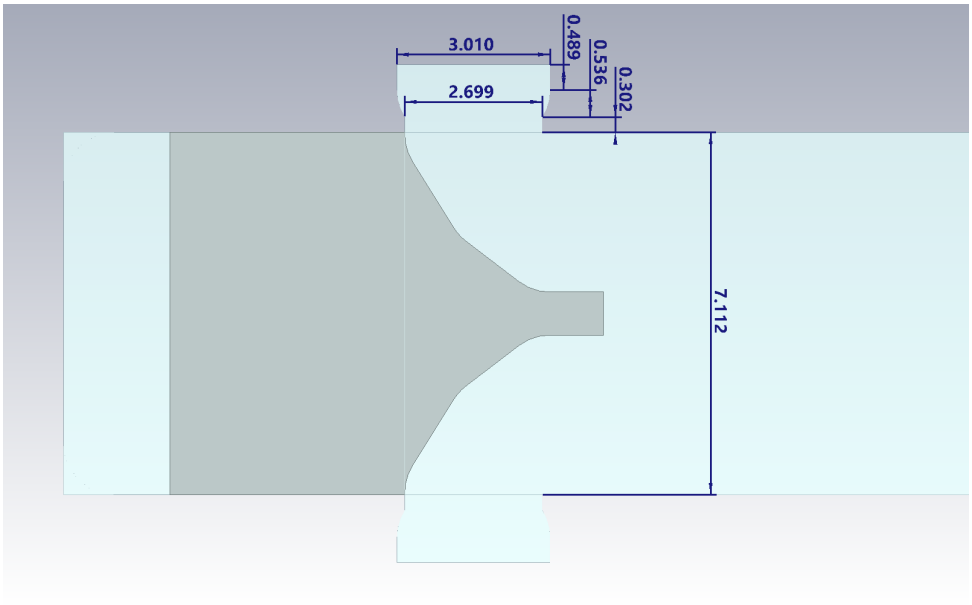

Figure 40: OMT base

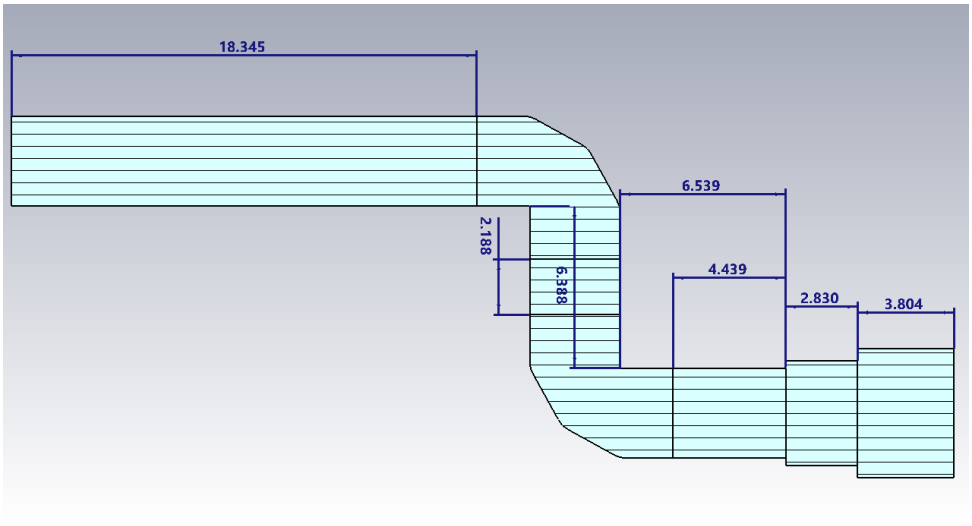

Figure 41: Axial port transformer

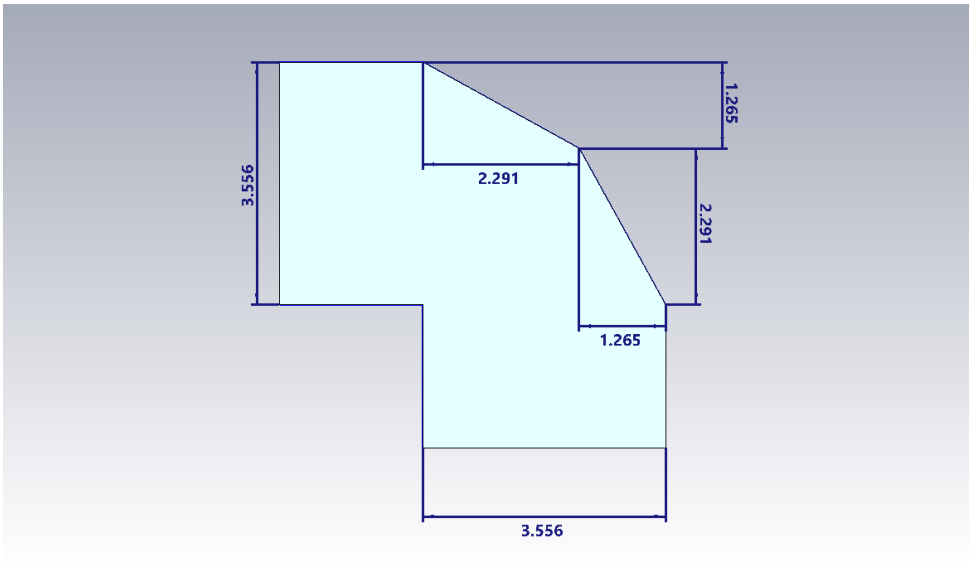

Figure 42: Axial port bend

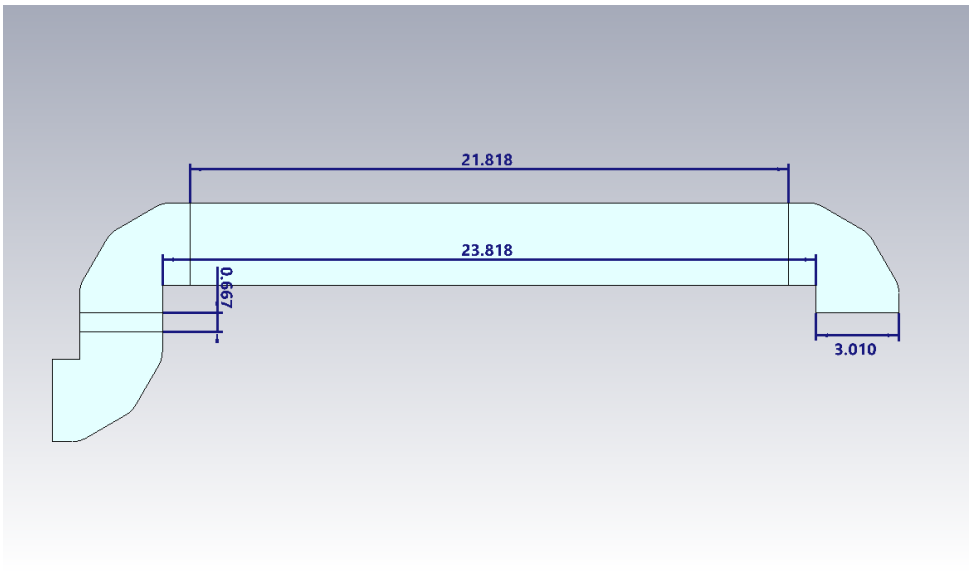

Figure 43: Sidearm

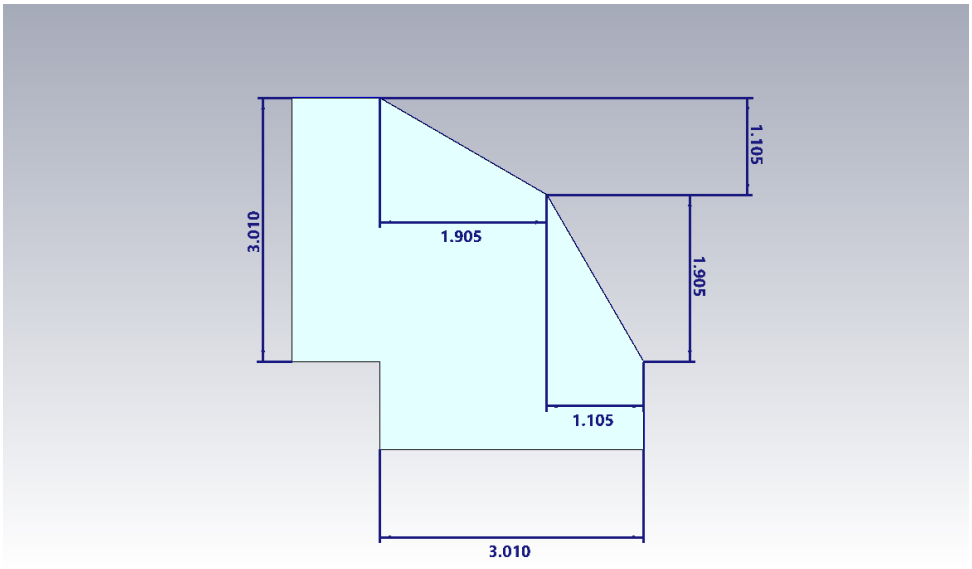

Figure 44: Sidearm bend

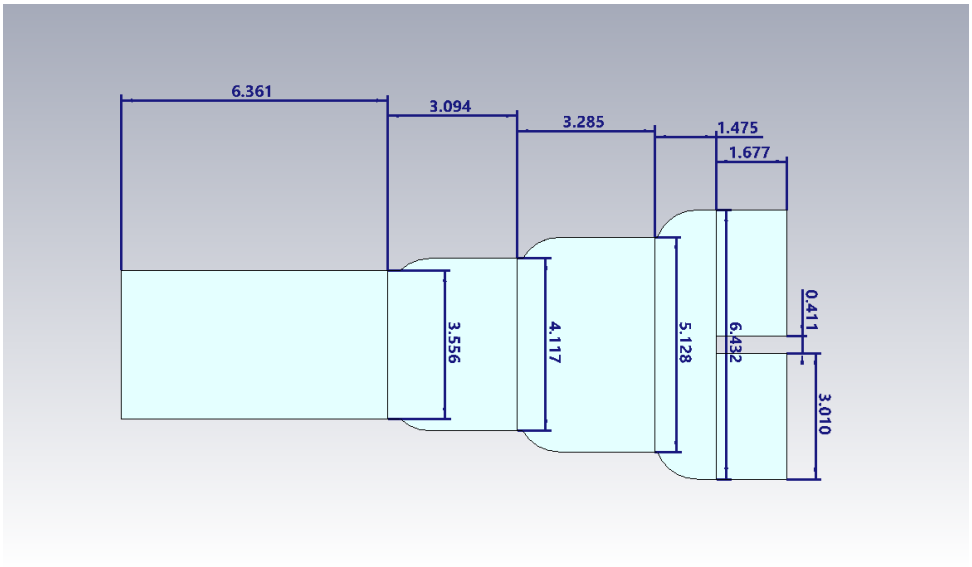

Figure 45: Sidearm combiner